10/3-14-94 9480 (1)

SANDIA REPORT

SAND92–2891 • UC–126
Unlimited Release
Printed February 1994

Long-Term Sealing Analyses for US Strategic Petroleum Reserve (SPR) Caverns

Brian Ehgartner

Prepared by
Sandia National Laboratories
Albuquerque, New Mexico 87185 and Livermore, California 94550
for the United States Department of Energy
under Contract DE-AC04-94AL85000

Issued by Sandia National Laboratories, operated for the United States Department of Energy by Sandia Corporation.

Available to DOE and DOE contractors from
Office of Scientific and Technical Information
PO Box 62
Oak Ridge, TN 37831

Prices available from (615) 576-8401, FTS 626-8401

Available to the public from
National Technical Information Service
US Department of Commerce
5285 Port Royal Rd
Springfield, VA 22161

NTIS price codes
Printed copy: A04
Microfiche copy: A01

SAND92-2891
Unlimited Release
Printed February 1994

Distribution
Category UC-126

Long-Term Sealing Analyses For US Strategic Petroleum Reserve (SPR) Caverns

Brian Ehgartner
Underground Storage Technology Department
Sandia National Laboratories
Albuquerque, New Mexico

ABSTRACT

It is inevitable that sealing and abandonment will someday occur in a SPR cavern or caverns. To gain insight into the long-term behavior of a typical SPR cavern following sealing and abandonment, a suite of mechanical finite-element calculations was performed. The initial analyses predict how quickly and to what extent a cavern pressurizes after it is plugged. The analyses also examine the stability of the cavern as it changes shape due to the excessive pressures generated as the salt creeps and the brine in the cavern thermally expands. These large-scale analyses do not include the details of the plug but assume a good seal is established in the cavern wells. In another series of analyses, the potential for forming a leak at the plug is evaluated. A cement plug, emplaced in the casing seat of a cavern well, is loaded using the predicted brine pressures from the cavern analyses. The plugged casing analyses examine the potential for forming a leak path in and along the interfaces of salt, casing, and cement plug. In the last set of analysis, the dimensional scale of the problem is further reduced to examine a pre-existing crack along a casing/salt interface. The cracked interface is assumed to be fluid filled and fully pressurized by the cavern fluids. The analyses address the potential for the fluid path to extend upwards along a plugged casing should an open microannulus surround the casing after it is plugged.

ACKNOWLEDGMENT

The author is appreciative to the reviewers of this report for the many constructive comments and criticisms. In particular Jim Todd, Jim Linn, and Rudy Matalucci served as primary reviewers. In addition, the analysis chapters (3 through 5) of this report were reviewed prior to assemblage of this report as technical memos written to Jim Linn and distributed internally to Sandia. The first such memo entitled "Predictions of Brine Pressure in a Sealed Cavern," 3/10/92, was reviewed by Tom Hinkebein. The second memo entitled "Response of a Plugged Casing to Pressures in Excess of Lithostatic," 6/17/92, was reviewed by Ray Finley. The third memo was entitled "Response of a Fluid-Filled Salt/Casing Interface to Pressures in Excess of Lithostatic," 7/15/92. That memo was reviewed by Steve Bauer. Cavern drawdown simulations using the SANSMIC code were performed by Phil Kuhlman and Tony Russo. These calculations provided the necessary information to calculate the changes in cavern pressure due to leaching after a cavern is plugged .

CONTENTS

FIGURES

TABLES

1.0 INTRODUCTION

The Strategic Petroleum Reserve (SPR) was created to reduce the vulnerability of the United States to interruptions by foreign oil suppliers. Approximately 570 million barrels of crude oil are presently stored underground in salt domes at five sites located along the Gulf of Mexico. One underground mine and approximately 60 leached caverns are used to store the oil.

It is inevitable that sealing and abandonment will someday occur in an SPR cavern or caverns. A simplistic view of a sealed SPR cavern is shown in Figure 1-1. To gain insight into the long-term behavior following sealing, a series of three finite-element analyses were performed. The analyses were purely mechanical and did not simulate fluid flow. Therefore, the calculations do not quantify the performance of a plugged cavern from a leakage point of view. To do so would require as a minimum a coupled mechanical-hydrological model that contains the appropriate deformational and fluid flow mechanisms. Rather, the evaluations presented in this report establish trends from the predicted time-dependent mechanical behavior of the cavern and plug area that are either favorable or unfavorable for sealing. For example, the sealing materials and salt are examined for tensile stresses that may fracture or separate the seal system and thus create or extend a flow path. Predicted deformation histories can also indicate whether sealing materials and their interfaces are tightening or becoming loose with time. From the predicted mechanical behaviors, the ability to seal an SPR cavern can be partially evaluated. Common to the analyses was a salt constitutive model (Chapter 2) that simulates the time-dependent creep of salt.

The initial analyses (Chapter 3) predict how quickly and to what extent a cavern pressurizes after it is plugged. The calculations also examine the stability of the cavern as its changes shape due to the excessive pressures generated due to salt creep and thermal expansion of the brine in the cavern. The effects of salt dissolution on cavern pressure are also quantified.

In another set of analyses (Chapter 4), the predicted brine pressures from the cavern analyses are applied to the bottom of a plugged casing. The plugged casing analysis examines the changes in borehole deformation and stress state as that area pressurizes over lithostatic pressure. The potential for forming a leak path in or along the salt, casing,

and cement plug are discussed along with the sensitivity of the results to changes in casing seat dimensions and bonding to the salt.

In the last analyses (Chapter 5), the scale of the problem is further reduced to examine a pre-existing crack or separation along a casing/salt interface. A portion of the interface is pressurized using the predicted fluid pressures from the cavern calculations to address the potential for growth of the fluid path along the interface. Both competent and deteriorated interfaces are simulated.

Each of the analysis Chapters introduce the problem, describe the finite-element model, and then discuss the results of the simulations. The report is concluded in Chapter 6.

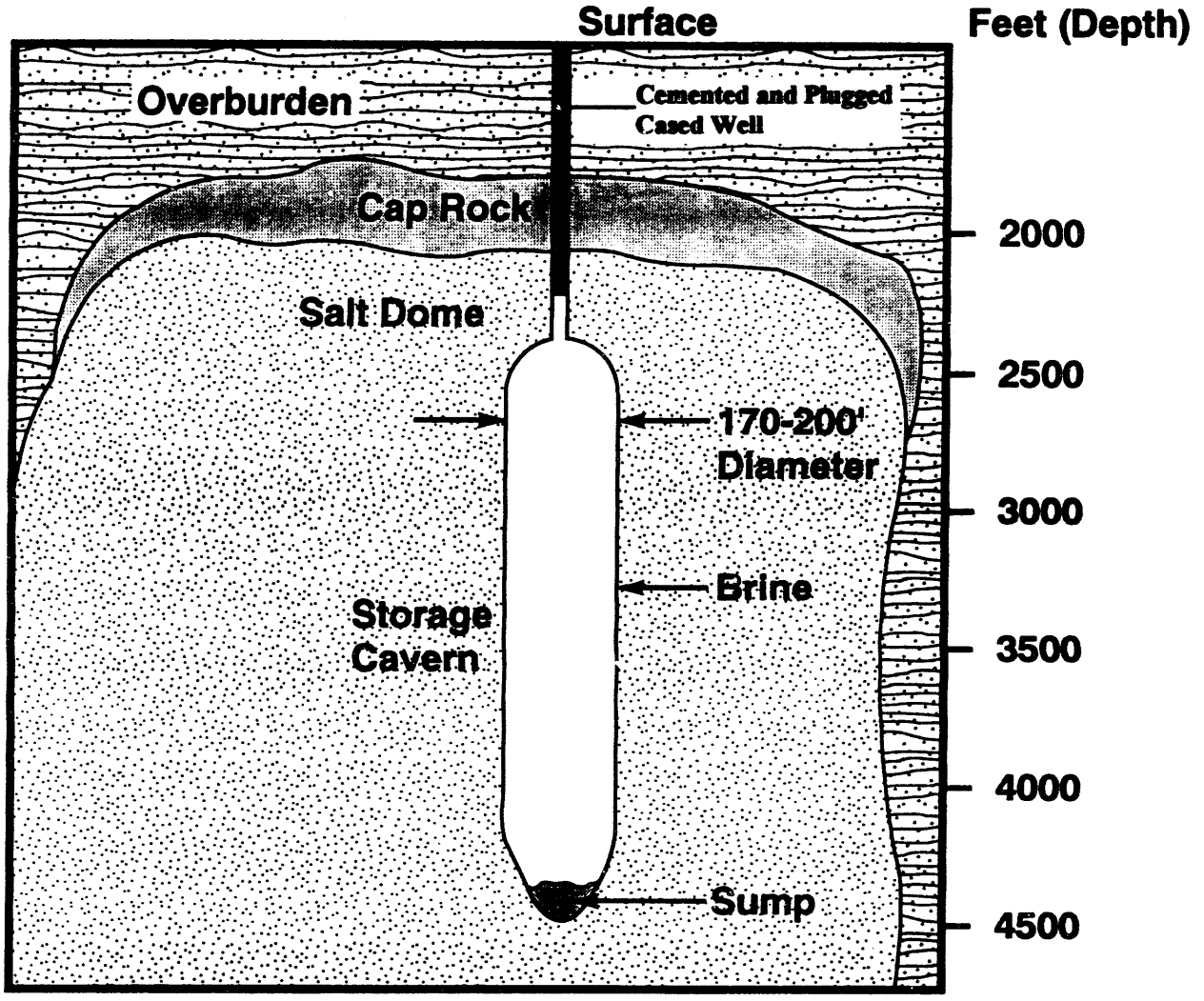

Figure 1-1. Plugged and Abandoned SPR Storage Cavern

2.0 CONSTITUTIVE MODELS

In this chapter, constitutive models and properties are described for the salt, steel casing, and cement simulated in the analyses in Chapters 3 through 5.

2.1 Salt

The mechanical behavior of the salt was represented by the Munson-Dawson creep model. The model is state-of-art in predicting salt behavior using a first principles approach. The model was developed for the Waste Isolation Pilot Plant (WIPP) Project and has been used to model a wide variety of underground structures and openings in salt at that site (Ehgartner 1990, 1991). The WIPP, located in southeastern New Mexico, is a excavated room-and-pillar facility designed for underground disposal of transuranic wastes in bedded salt.

The model has been validated with underground deformation data from a variety of opening shapes and sizes at the WIPP. (Munson, Fossum, and Senseny, 1989a,b; Munson and DeVries, 1990; Munson, et. al.,1992). For SPR problems, predicted surface subsidence and cavern pressurization rates agree well with those measured at West Hackberry (Ehgartner, 1992).

The model is a Multimechanism Steady-state Workhardening/Recovery Model as originally developed by Munson and Dawson (1979) and later modified to provide a more descriptive transient strain function (Munson, Fossum, and Senseny, 1989a,b). The model incorporates the Tresca flow potential and is based on micromechanistic concepts using a deformation mechanism map (Munson, 1979). The mechanism map defines regions of stress and temperature in which a unique deformation mechanism controls or dominates steady-state creep. The model identifies three steady-state mechanisms. The total steady-state strain rate is simply the sum of the strain rates of each individual mechanism.

$$\dot{\varepsilon}_s = \sum_{1}^{3} \dot{\varepsilon}_{s_i}$$

The equations describing each of the individual steady-state mechanisms follow. Mechanism 1 (dislocation climb) dominates at high temperatures and low stresses. Mechanism 2 (undefined) controls creep at low temperatures and stresses, and Mechanism 3 (dislocation glide) dominates at high stresses at all temperatures.

$$\dot{\varepsilon}_{s_1} = A_1 \, e^{-Q_1/RT} (\sigma/\mu)^{n_1}$$

$$\dot{\varepsilon}_{s_2} = A_2 \, e^{-Q_2/RT} (\sigma/\mu)^{n_2}$$

$$\dot{\varepsilon}_{s_3} = |H| \, [B_1 e^{-Q_1/RT} + B_2 e^{-Q_2/RT}] \sinh[q(\sigma - \sigma_0)/\mu]$$

Each of the above mechanisms relates the steady-state strain rate to temperature, T, and stress, σ. The constants A, n, Q were determined from laboratory creep tests, where Q is the activation energy and n is the stress exponent. R is the universal gas constant and μ is the shear modulus of salt. |H| is the Heaviside step function with argument of $(\sigma-\sigma_0)$. The basic form of the creep law for steady-state Mechanisms 1 and 2 is similar to that used in most previous analyses for both the Waste Isolation Pilot Plant (WIPP) and the SPR (Krieg, 1984).

Transient creep is included in the model through a function, F, which relates the transient strain rate to the steady-state strain rate in the following function:

$$\dot{\varepsilon} = F \, \dot{\varepsilon}_s$$

The transient function, F, is composed of a workhardening, equilibrium, and recovery branch.

$$F = \begin{cases} e^{\Delta(1-\zeta/e_t)^2} & \text{Workhardening} \\ 1 & \text{Equilibrium} \\ e^{-\delta(1-\zeta/e_t)^2} & \text{Recovery} \end{cases}$$

Δ and δ are workhardening and recovery parameters and e_t is the transient strain limit. The equation governing the rate of change of the internal variable, ζ, is

$$\dot{\zeta} = (F - 1)\,\dot{\varepsilon}_s$$

The transient strain limit is related to stress and temperature, T, through the following function where K_0, c, and m are constants.

$$e_t = K_0\, e^{cT} (\sigma / \mu)^m$$

The workhardening and recovery parameters are defined as a function of stress through

$$\Delta = \alpha_w + \beta_w \log(\sigma / \mu)$$
$$\delta = \alpha_r + \beta_r \log(\sigma / \mu)$$

where the α's and ß's are constants with the subscripts denoting either the workhardening or recovery branches.

Table 2-1
Mechanical Properties of West Hackberry Salt

Elastic Properties

Poisson's Ratio	0.25
Modulus of Elasticity (E)	4.5×10^6 psi

Creep Properties*

Steady-state Mechanism 1		Steady-state Mechanism 2	
A_1	8.386 E22 /s	A_2	1.290 E12 /s
Q_1	25000 cal/mol	Q_2	12000 cal/mol
n_1	5.5	n_2	4.9
Steady-state Mechanism 3		**Transient Creep**	
B_1	6.086 E6 /s	m	3.0
B_2	3.034 E-2 /s	K_0	6.275 E5
σ_o	2985 psi	c	0.009198 /T
q	5.335 E3	α_w	-17.37
		β_w	-7.738
		α_r	1.05
R	1.987 cal/mol-deg	β_r	0.0

* Steady-state constants A_2, Q_2, n_2 for Mechanism 2 were estimated from laboratory creep tests (Wawersik and Zeuch, 1984). Steady-state parameters for Mechanisms 1 and 3, and transient parameters were taken from the WIPP data base (Munson, 1989a) for pure halite. Steady-state mechanism 1 and 3 should have a minor effect on the creep predicted in this report according to the mechanism map.

2.2 Casing and Cement

In addition to salt, the analyses in Chapters 4 and 5 simulate steel casings and cement. These materials are assumed to behave elastically. The properties of the steel casing and cement are listed in Table 2-2.

Table 2-2
Properties of Casing and Cement

	Modulus of Elasticity (psi)	Poisson's Ratio
Steel Casing	29×10^6	0.30
Cement Annulus and Plug	3.8×10^6	0.19

The casing properties represent a K55 steel. The casing simulated in the analyses has a weight of 133 lb/ft and a wall thickness of 5/8 inches. The cement properties approximate a fine grade cement with a water/cement ratio of 0.4 and a cement/aggregate ratio of 0.5 with an unconfined compressive strength of 3625 psi. Technically, the mixture is a concrete, yet it is commonly referred to as a cement.

The SPECTROM-32 code (RE/SPEC, 1989), version 4.02, was used to perform the simulations. The code is a two-dimensional finite-element thermomechanical stress analysis program written to solve nonlinear, time-dependent rock mechanics problems. The salt constitutive model, successfully used in the validation exercises mentioned in the beginning of this section, is implemented into this code and was used to perform the majority of validation analyses for the WIPP.

3.0 SEALED CAVERN ANALYSES

3.1 Introduction

Several factors influence the pressure history of brine contained within a sealed SPR cavern-- salt creep, brine temperature changes, and salt dissolution. These factors are briefly discussed below, then the finite element method is used to model them and predict the brine pressure history in a sealed SPR cavern.

Creep is an ongoing process that continues after a cavern is sealed as long as the cavern has a vertical dimension. As a result of differences in density between brine and salt, a differential pressure gradient (and hence creep) will exist between the brine and salt. Brine has a density that results in a pressure gradient of approximately 0.52 psi/ft of depth, whereas salt has a pressure gradient of approximately 0.94 psi/ft of depth. This results in a pressure differential of 0.42 psi/ft of depth. Creep should cause the brine pressure to increase with time. At some point however, the brine pressure in the upper portion of the cavern is expected to exceed lithostatic stress and the top portion of the cavern will expand. When the rate of volumetric expansion in the upper portion of the cavern approaches that of contraction in the lower portion of the cavern, the rate of brine pressurization will approach zero and the cavern brine pressure is assumed to reach equilibrium. This pressure state is illustrated in Figure 3-1. This definition of equilibrium will suffice for purposes of this report because appreciable changes are not predicted in the vertical dimension of a sealed cavern within the time frame evaluated here (up to 1000 years). However, as alluded to above, geologic time scales will permit the cavern to completely close at the bottom, thereby changing the equilibrium pressure as the bottom depth of the cavern is redefined.

Brine temperature changes result from the heat exchange between the salt in the cavern walls and cavern brine. Prior to sealing and abandonment, fresh water or brine will be injected into the caverns to remove the oil. Because the injected fluid temperature is typically less than the cavern walls, heating of the fluid will result in fluid expansion and pressure buildup over time after the cavern is sealed. Pressurization due to heat exchange will slow as the average brine temperature approaches the average salt temperature. The heat transfer mechanisms and thermal modeling associated with SPR caverns is discussed by Tomasko (1985).

Salt dissolution will occur as a consequence of injecting fresh water or partially saturated brine into cavern during removal of oil. Even if the brine were fully saturated when injected, its heating due to contact with the cavern walls would allow an increase in the solute content of the brine and therefore some dissolution. Salt dissolution creates additional cavern space and brine volume. However, the volume leached is slightly greater than the increase in brine volume that occurs. This will result in a decrease in the brine pressure. From a chemistry viewpoint, the bonding between the water molecules and the sodium-chloride ions results in a solution volume that is smaller than the total volumes of the constituents. The net increase in space available for the brine results in a decrease in pressure according to the compressibility factor of the brine. Because brine saturation is a function of temperature and pressure, the salinity will to a small extent dependent upon the thermal exchanges and creep.

Understanding the factors that control the fluid pressure history in a sealed cavern is necessary for predictive modeling. The model predictions in this chapter will stand alone and be used as input in Chapters 4 and 5 analyses to evaluate the potential for leakage of a plugged and abandoned SPR cavern. A leak path could form when the fluid pressure in the cavern exceeds the lithostatic pressure of the salt. This pressure condition occurs in the upper portion of the cavern after sealing and abandonment and the pressure differential will be greatest at the casing seat. The response of a plugged casing seat is investigated in Chapter 4. If a leak path is formed at the casing seat, it may progress upwards with time along the salt/casing interface because the pressure differential between the brine and salt increases with elevation. This topic is investigated in the interface calculations presented in Chapter 5.

In this chapter, the influence of creep, heat exchange, and dissolution in a sealed cavern are investigated using the finite element method. A coupled creep-thermal-dissolution model is used to predict the brine pressure history at the casing seat of typical SPR cavern. The results can be used to improve engineering decisions regarding cavern abandonment and sealing. For example, the salinity and temperature of the injection fluid and seal emplacement time may be controlled to provide more favorable pressure conditions in the cavern for sealing purposes.

3.2 Finite-Element Model

Cavern behavior was simulated for 1000 years to capture the long-term response of a sealed cavern. The baseline finite-element model used for the initial 30 years of simulation is described in detail by Ehgartner (1992). The model is intended to represent a typical SPR cavern field. Basically the cavern field consists of a network of 2000 ft high by 170 ft diameter caverns spaced at 750 ft (center-to-center). The top of the cylindrical shaped caverns is at a depth of 2500 ft below the ground surface and 500 ft into the salt. The salt is overlaid with 400 ft of caprock (typ. anhydrite) and 1600 ft of overburden (typ. sand). The salt properties were described in Chapter 2 and are based in part on elastic and creep tests of West Hackberry salt. The predicted results of the baseline model closely agreed with measured surface subsidence and cavern pressurization rates at West Hackberry thus providing some verification and credibility to the model.

The cavern was assumed to be filled with oil for the first 30 years. Thirty years is the projected operating life initially assigned to SPR caverns. Because the actual number of drawdowns (oil withdrawals) to date is less than designed for, the operating life of most caverns may eventually be extended. This should have a minor impact of the conclusions drawn in this report, because the cavern pressurization rates will decrease by only a small amount as the cavern ages past 30 years (Hoffman, 1992). A depth-dependent pressure gradient was applied to the cavern boundary to account for the weight of the oil and an average operational oil pressure of 680 psi at the wellhead. An oil pressure of 680 psi is a typical average for the cavern field simulated and represents an oil/brine interface at the bottom of the caverns. After 30 years, a complete drawdown of the oil in the cavern was simulated. The oil pressure boundary was replaced with brine pressure equivalent to 0 psi at the wellhead. The pressure change was simulated as occurring instantaneously, whereas in reality it will take some time to replace the cavern oil with brine. It was estimated (Kuhlman and Russo, 1992) that approximately 0.29 years will be required to completely empty the cavern. At 30.29 years, the cavern is assumed to be full of brine and instantaneously plugged. At that time, the cavern brine was simulated using special fluid elements.

Prior to cavern sealing, cavern fluids were not explicitly modeled, rather they were represented as pressure gradients applied to the boundaries of the cavern. Once the cavern is plugged, the cavern pressures are not controllable at the wellhead, but determined by the mechanisms discussed above. For example, the brine exerts a

backpressure on the salt dependent upon the amount of compression due to cavern closure. The brine elements modeled a compressible, inviscid fluid with a bulk modulus of 3.46×10^5 psi and density of 1.20 g/cc. These properties remained constant throughout the analysis. The finite-element mesh is shown in Figure 3-2a,b-- before and after emplacement of the special fluid elements at 30.29 years. The cavern casings and plug are not included in the analysis, but are considered as separate analyses in the chapters to follow. The two-dimensional axisymmetric analyses rotate the mesh about the cavern centerline and constrain radial displacements on the outer edge of the mesh (rollered boundary conditions) to approximate an infinite number of caverns in a field (Ehgartner, 1992).

Creep was modeled in all the analyses performed. In some of the analyses, the thermal history of brine was simulated by assigning a prescribed temperature history to the brine. For this purpose, the average oil temperatures measured at Bryan Mound and fitted to a general expression by Todd (1991) was used. The following temperature history was assigned to the brine after plugging of the cavern:

$$T = T_{inf} - (T_{inf} - T_o)\, e^{(-t/Tau)}$$

where T is the time dependent temperature (°F), T_{inf} is the temperature at infinity (124 °F), T_o is the initial temperature (107 °F), t is the time (yrs) after cavern sealing, and Tau is a constant (6.6 yrs). T_{inf} represents the in situ temperature of salt at a depth of 3500 ft (cavern mid-height). The thermal expansion of brine was assumed to be constant at 1.54 E-4 1/°F and salt temperatures were not changed in the finite-element model. In reality the local salt temperatures will slightly decrease as the brine geothermally heats.

Salt dissolution was simulated by assigning an equivalent temperature drop to the brine based on the net volumetric change of the cavern and brine. As discussed earlier, dissolutioning creates slightly more cavern volume than brine volume. This approach is artificial because brine temperatures are reduced in the model to account for volume reductions. Salt temperatures remain unchanged. This approach enables the dissolution response to be simulated without actually replacing salt elements in the model with brine

elements and imposing a reduced pressure on them. However, the cavern geometry in the model is unaffected by the dissolutioning occurring during the drawdown. The increase in cavern diameter after a complete drawdown of a cavern averages approximately 10 %. This results in a small change in the shape of the cavern, but the cavern is still relatively long in comparison to its new diameter (L/D > 10:1). Because the volumetric creep rate (normalized to volume) of a very long cavern is independent of the diameter of the cavern, the new cavern geometry is assumed to have a negligible effect on the brine pressurization rate in the cavern.

SANSMIC (Russo, 1983) was used to calculate the volume change due to dissolution following a complete drawdown of the cavern (Kuhlman and Russo, 1992). In this calculation, fresh water was injected into a typical SPR cavern. The drawdown was completed in 106 days (0.29 yrs) and dissolution continued for a additional 120 days (0.33 yrs) after the drawdown. The net volumetric change of the system was converted to an equivalent temperature drop using the coefficient of thermal expansion for brine. The cavern was assumed to be plugged immediately following the drawdown (30.29 yrs) to maximize the pressure drop due to dissolutioning. Changes in salinity due to changes in brine temperature and pressure were assumed to be negligible.

The casing seat was assumed to be located 100 ft above the roof of the cavern. The open uncased wellbore between the casing seat and cavern is sometimes referred to as the chimney. At the casing seat depth (2400 ft), the lithostatic pressure was calculated as 2110 psi, based on the density and thickness of the overlying layers in the baseline model discussed above. The cavern chimney was not modeled in the calculations as its relatively small volume will have a minor effect on the overall pressurization rates for the cavern. Brine pressure was estimated at the casing seat based on the density of the brine (0.52 psi/ft) and predicted brine pressures in the cavern. This assumes the chimney volume is open and the plugged casing forms an impervious seal. At the time of plugging, the brine pressure at the casing seat is assumed to be 1250 psi, based on the density of brine to the surface and no additional wellhead pressure.

The modeling approach used in this study differs significantly from that used in previous cavern sealing calculations. Previous sealed cavern calculations for the SPR (Preece, 1985) modeled the brine as static pressure based on an assumed long-term equilibrium with lithostatic pressure. Thus the pressure history between the time of sealing and the time required to reach creep equilibrium was not simulated. This was necessary as the

codes at that time did not have an element birth/death option to allow brine emplacement after the start of the calculation, and the constitutive model for a fluid element was not available in the codes at that time. Also, the previous calculations used a softened modulus of elasticity for the salt-- an adjustment that enabled better matches to measured salt deformations. The effects of dissolution and thermal heating of the brine on cavern pressure were not modeled in past studies.

3.3 Results

Figure 3-3 shows the effect of creep and salt dissolution on brine pressure at the casing seat after plugging of the casing. As discussed earlier, the cavern was plugged immediately following drawdown of the cavern. For comparative purposes, the initial brine pressure at the time of plugging is shown. The upper curve in the Figure represents the response of the cavern fluid to creep. When only creep is considered (no dissolution), the cavern pressurizes after sealing. The effect of including dissolution was to initially lower pressures after sealing (see lower curve). Since cavern sealing immediately followed the complete removal of oil from the cavern by brine displacement, residual leaching or dissolution after sealing was maximized. Dissolution after cavern sealing resulted in a depressurization of approximately 700 psi within 1 month. At one month after cavern sealing, the rate of volumetric decrease due to leaching approximately equals the volumetric closure rate due to creep. Thereafter, creep dominates the volumetric response of the cavern resulting in a pressure increase. The pressure difference between the creep and creep-dissolution models amounts to approximately 700 psi at the end of the 120 day dissolution period.

Figure 3-4 shows the effect of geothermal heating of the brine pressure in a sealed cavern. Creep was included in the analysis, however dissolution effects were not simulated. For comparative purposes, the lithostatic pressure at the casing seat and the predicted response of modeling only creep are shown. The pressure buildup, resulting from thermal heating of brine, results in an overpressurization at the casing seat within 2.1 years after sealing. Overpressurization is defined when the fluid pressure exceeds the lithostatic pressure of the salt at that level. The predicted thermal pressure peaks at about 15 years after increasing over 1800 psi from the initial 1250 psi brine pressure at the casing seat. The rate of pressure increase during this time decreases, thus implying that the creep response of the salt is more able to accommodate the geothermally driven expansion of

brine with time. As shown earlier, the geothermal heat exchange of salt with brine decreases with time. At later times, the brine pressure decreases with time as the cavern is over-pressurized and additional pressure contributions due to geothermal heating are small. In contrast to the creep-thermal model, the creep only model predicts a relatively modest pressure increase resulting in a pressure difference of approximately 1300 psi at 15 years after sealing.

Figure 3-5 shows the cavern deformations (magnified by 3) and salt velocity vectors at three different times for the heated brine analysis. A velocity vector indicates the direction of salt flow and relative particle velocity at a particular time. Prior to plugging, the salt flow is predominantly downward and into the lower portion of the cavern where the majority of deformation is predicted. Prior to plugging, closure is predicted at all locations in the cavern. One year after plugging, the cavern walls are expanding because the cavern fluid pressures are greater than the stresses in the salt. At this particular time, the cavern fluid pressure is approaching, but still less than lithostatic pressure. The cavern behavior up to this time may be dominated by the transient response of the salt due to the abrupt buildup of brine pressure. At later times, the thermal pulse has lessened and the cavern responds by establishing the long-term behavior where closure occurs in the bottom portion of the cavern, and expansion in the upper portion. This behavior is expected since the brine pressures at this time exceed lithostatic pressure in the top of the cavern, but are below the lithostatic pressure at the bottom of the cavern. The cavern response is largely controlled by steady-state creep at this time driven by the difference in pressure gradients between the brine and salt.

Although the caverns are predicted to enlarge in the roof area, the amount is small. For the heated brine analysis, the roof at 1000 years after plugging expanded in the horizontal directions less than 0.7 ft. The vertical uplift at the center of the roof is predicted to be 1.1 ft, 1000 years after plugging. Near the bottom of the cavern, closure is drastically slowed as the brine pressure raises after plugging. The additional strain accumulation in the salt is less than 1 percent during the 1000 years after plugging of the cavern. This is small increase compared to the estimated 15 percent strain that is typically required to fail salt under this stress state (Preece and Wawersik, 1984). The maximum amount of surface subsidence is predicted for the case where dissolution occurs following plugging and the brine pressurizes in the long term due to creep only. The relatively lower cavern pressures for this case result in approximately 1 ft of additional surface subsidence after 1000 years following plugging.

To further evaluate the stability of the cavern, the stresses in the salt were examined, particularly during the relatively rapid cavern enlargement period following plugging in the heated brine analysis. Of concern was the potential development of tensile stresses in the roof or walls of the cavern as the cavern enlarges. No tensile stresses were predicted in the salt at any time. However, the compressive stresses in the salt adjacent to the cavern decreased as the cavern initially enlarged. The minimum compressive stress in the roof of the cavern was 1760 psi at 2.5 years after plugging. The minimum compressive stress in the cavern walls was 1605 psi at the top of the cavern at 2.2 years after plugging. The brine pressure acting against the top portion of the cavern at these times was approximately 2250 psi or nearly equal to the lithostatic at that depth. After reaching minimum stresses at 2.5 and 2.2 years respectively, the roof and wall stresses became more compressive with time and remained slightly below brine pressures through the remainder of the analysis.

Figures 3-6 and 3-7 shows the brine pressure predictions for the creep, creep-thermal, creep-dissolution, and creep-dissolution-thermal models out to 50 and 1000 years, respectively. The thermal effect is most significant as noted by the separation between the thermal (upper two curves) and non-thermal (lower two curves) results. Dissolution is a secondary effect which results in an initial decrease in pressure for both thermal or non-thermal models. Later times show dissolution to result in a higher brine pressure for the thermal model and a lower pressure for the constant temperature model. Table 3-1 lists the predicted time to exceed lithostatic stress at the casing seat.

Table 3-1

Predicted Time for Cavern Brine Pressure to Reach Lithostatic Pressure

Model	Time to Lithostatic (yrs)
salt creep--thermal heating of brine	2.1
salt creep--salt dissolution--thermal heating of brine	3.8
salt creep	206
salt creep--salt dissolution	352

The thermal heating of the brine results in approximately a 100 fold decrease in the time to reach lithostatic pressure at the casing seat, whereas dissolution of salt following plugging results in approximately a 2 fold increase in the time to lithostatic pressure. The geothermal heating of brine not only results in a quicker time to exceed lithostatic pressure, but the peak pressures are much greater for the thermal models. As discussed earlier, when the brine pressure reaches the lithostatic pressure in the salt, a leak path can potentially form. These results necessitated the plugged casing and interface analyses in the following chapters.

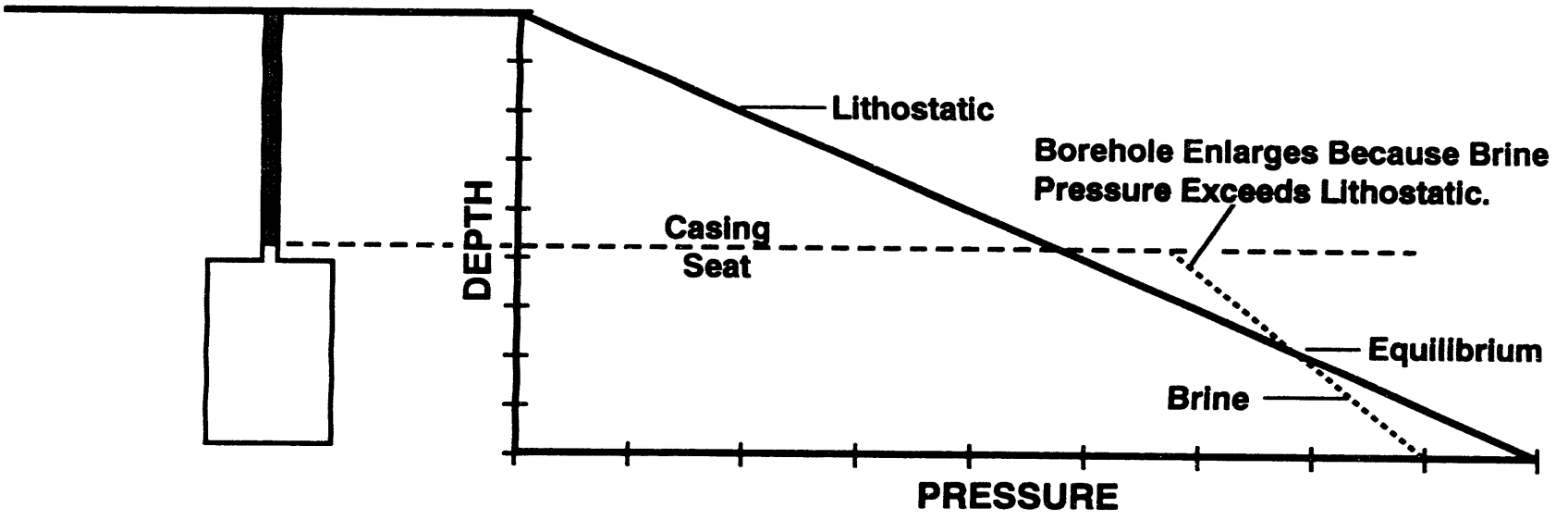

Figure 3.1. Illustration of Pressure Differential Between Brine and Lithostatic Pressure at the Casing Seat.

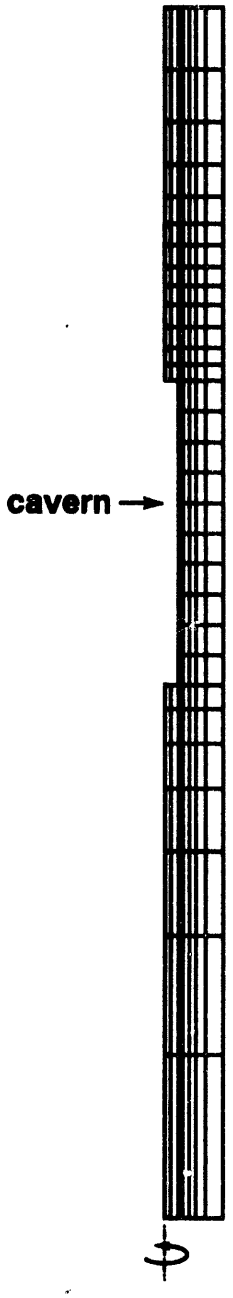

a) Prior To Brine Fill.

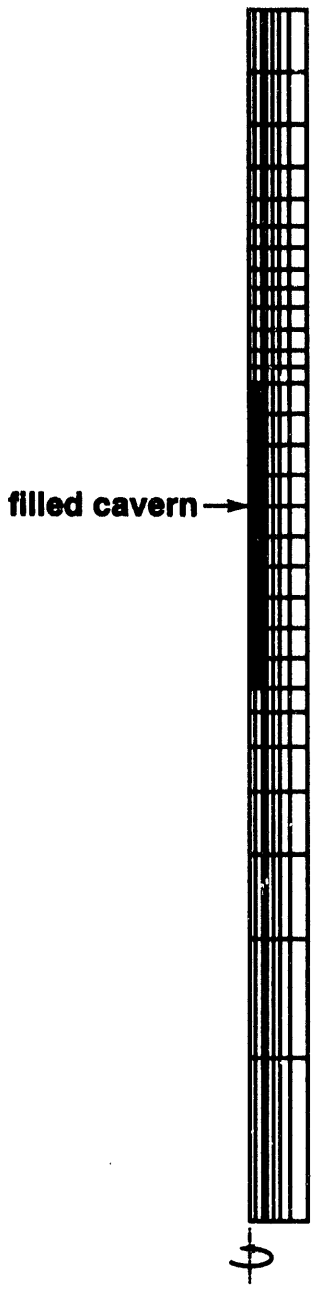

a) With Brine Elements.

Figure 3-2. Finite-Element Mesh Used in Sealed Cavern Analyses.

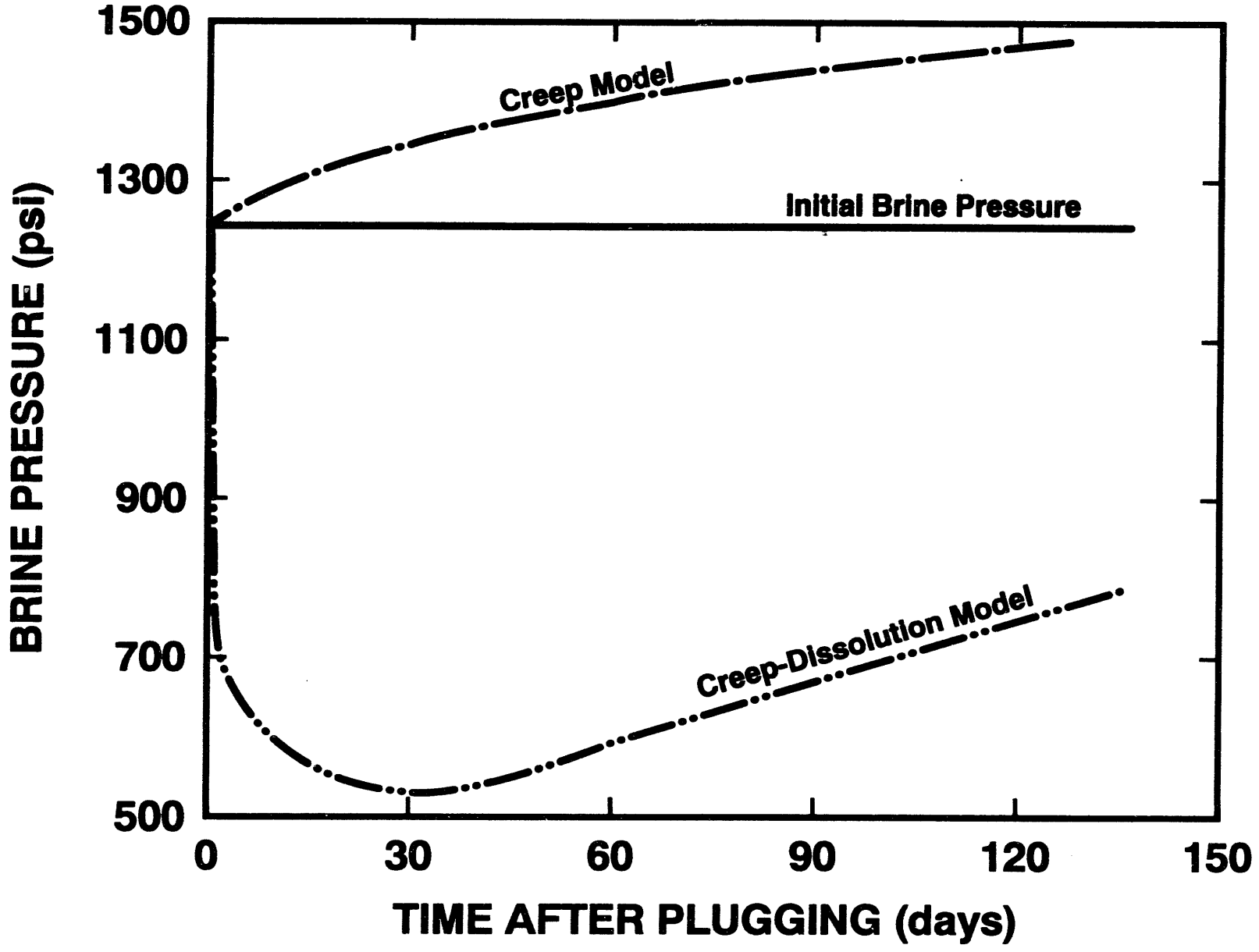

Figure 3-3. Effect of Salt Dissolution on Brine Pressure at Casing Seat.

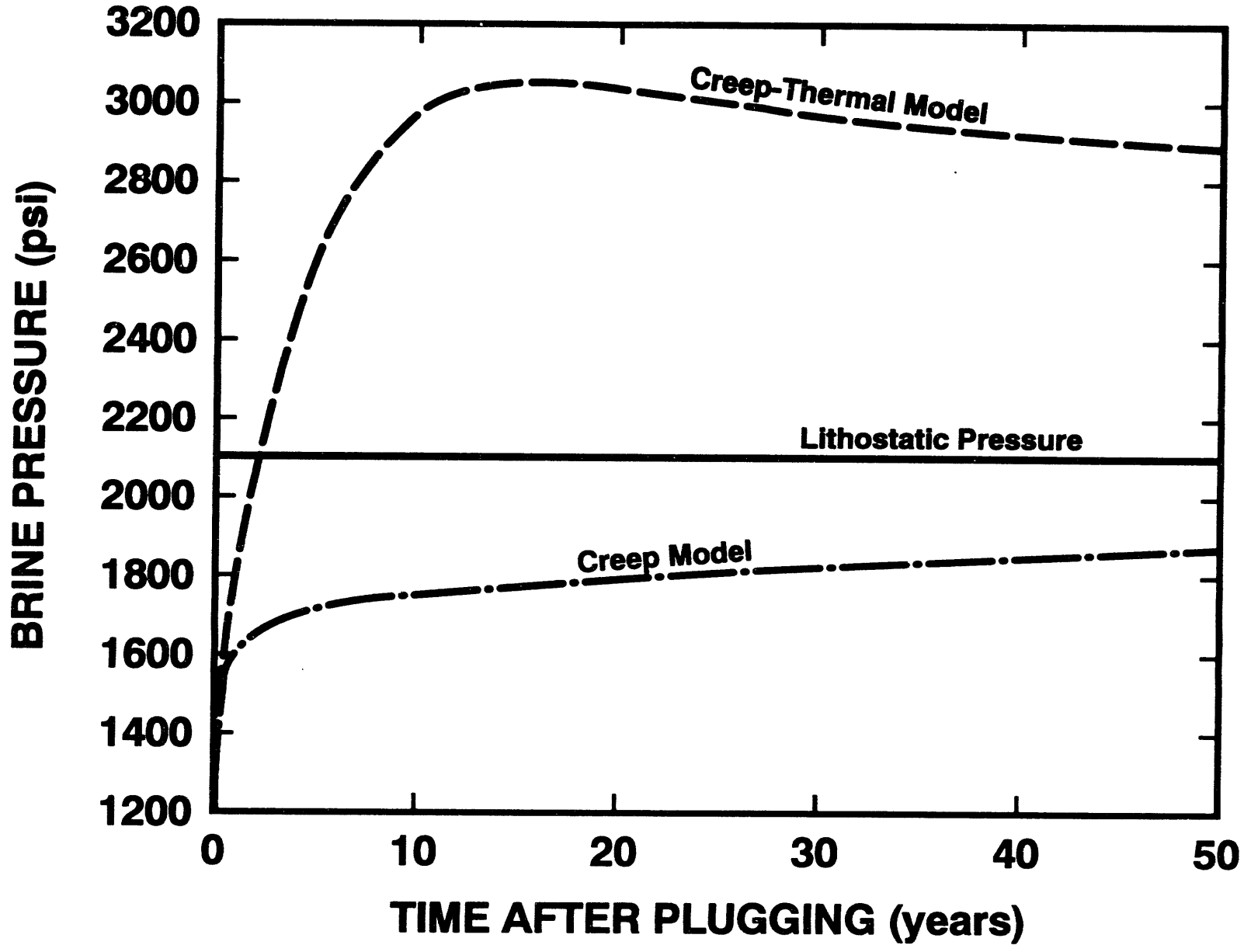

Figure 3-4. Effect of Brine Heating on Brine Pressure at Casing Seat.

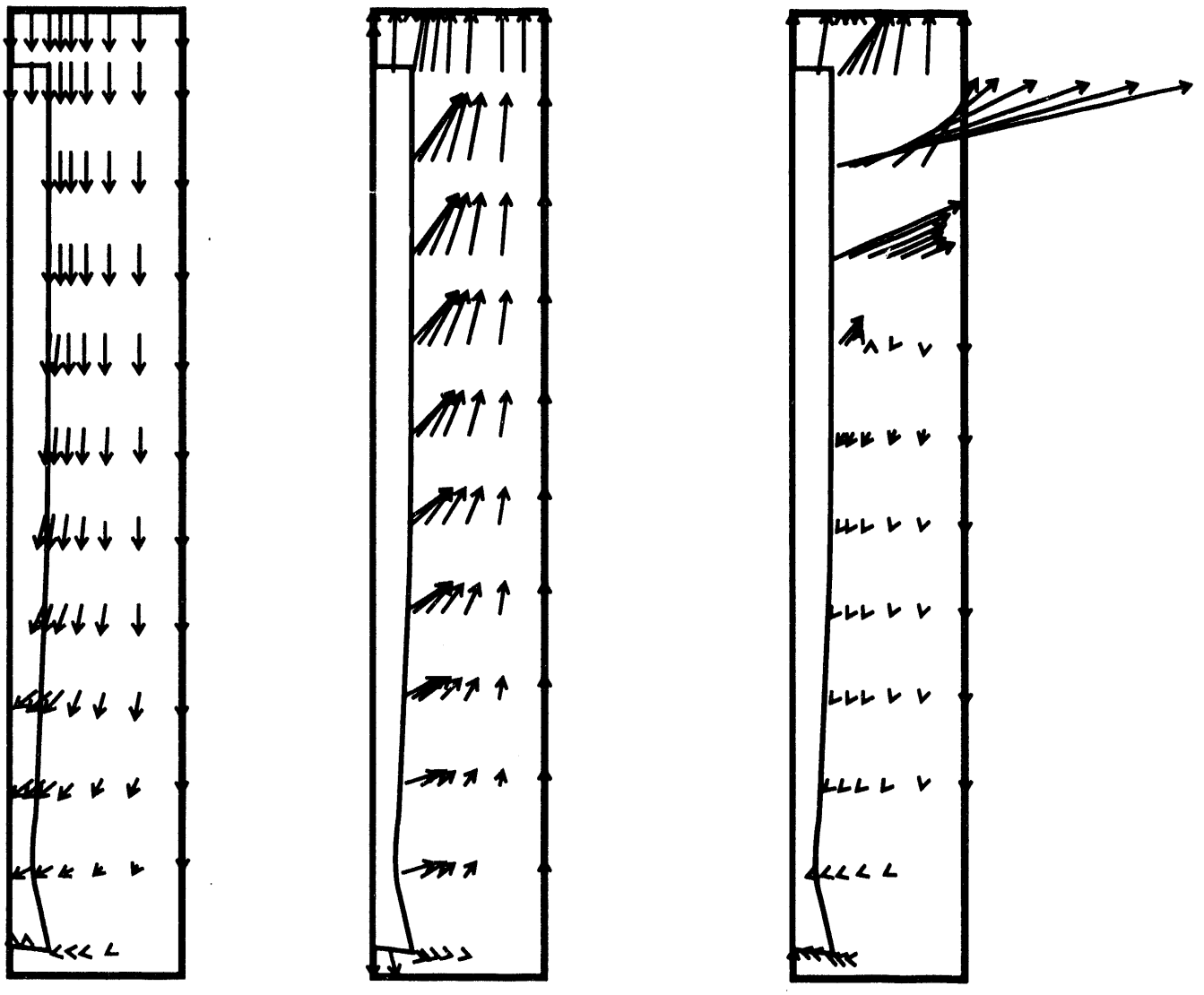

Figure 3-5. Cavern Deformation and Vector Plots During Brine Heating

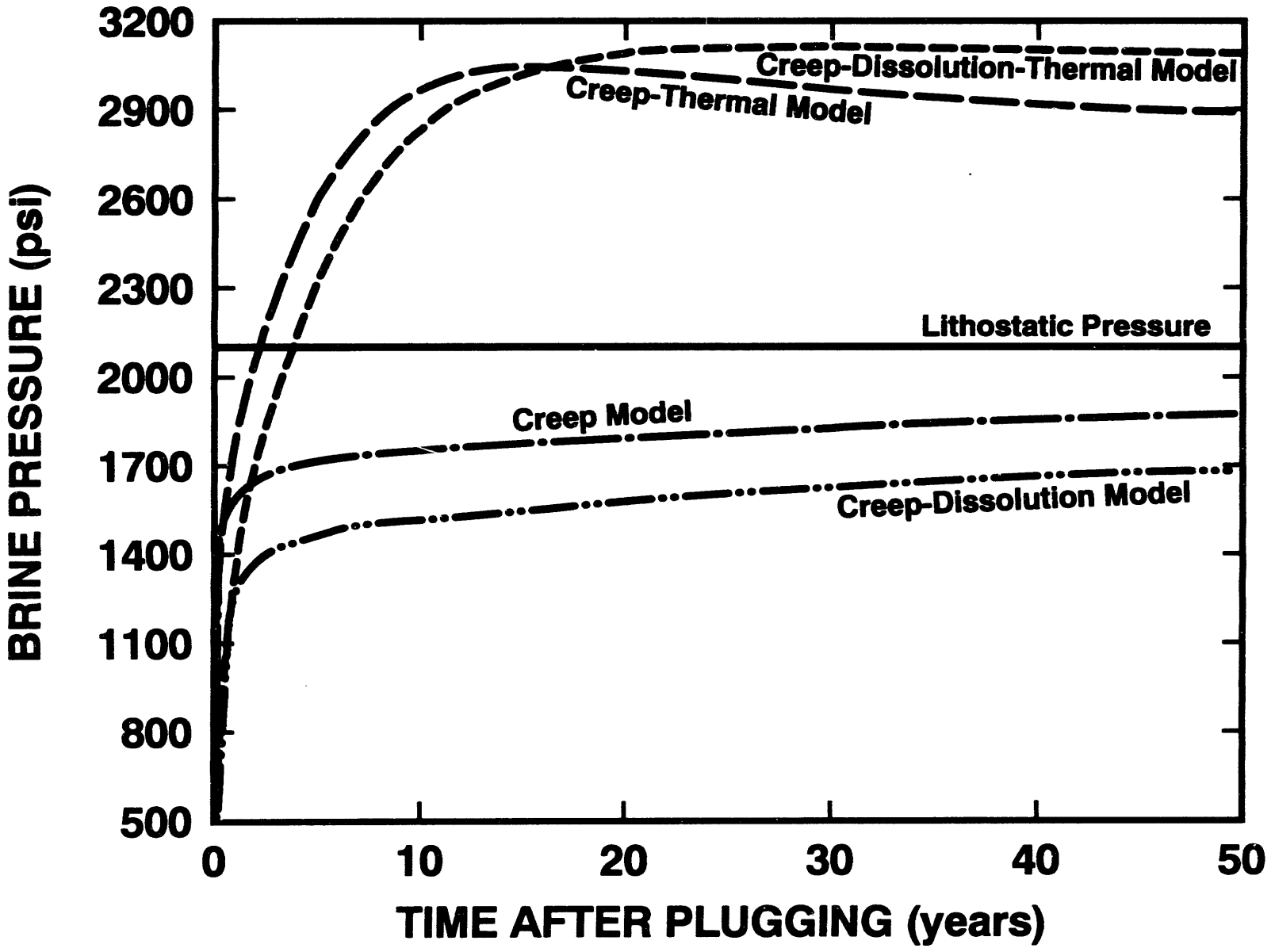

Figure 3-6. Coupled Model Predictions (0 to 50 yrs) of Brine Pressure at Casing Seat.

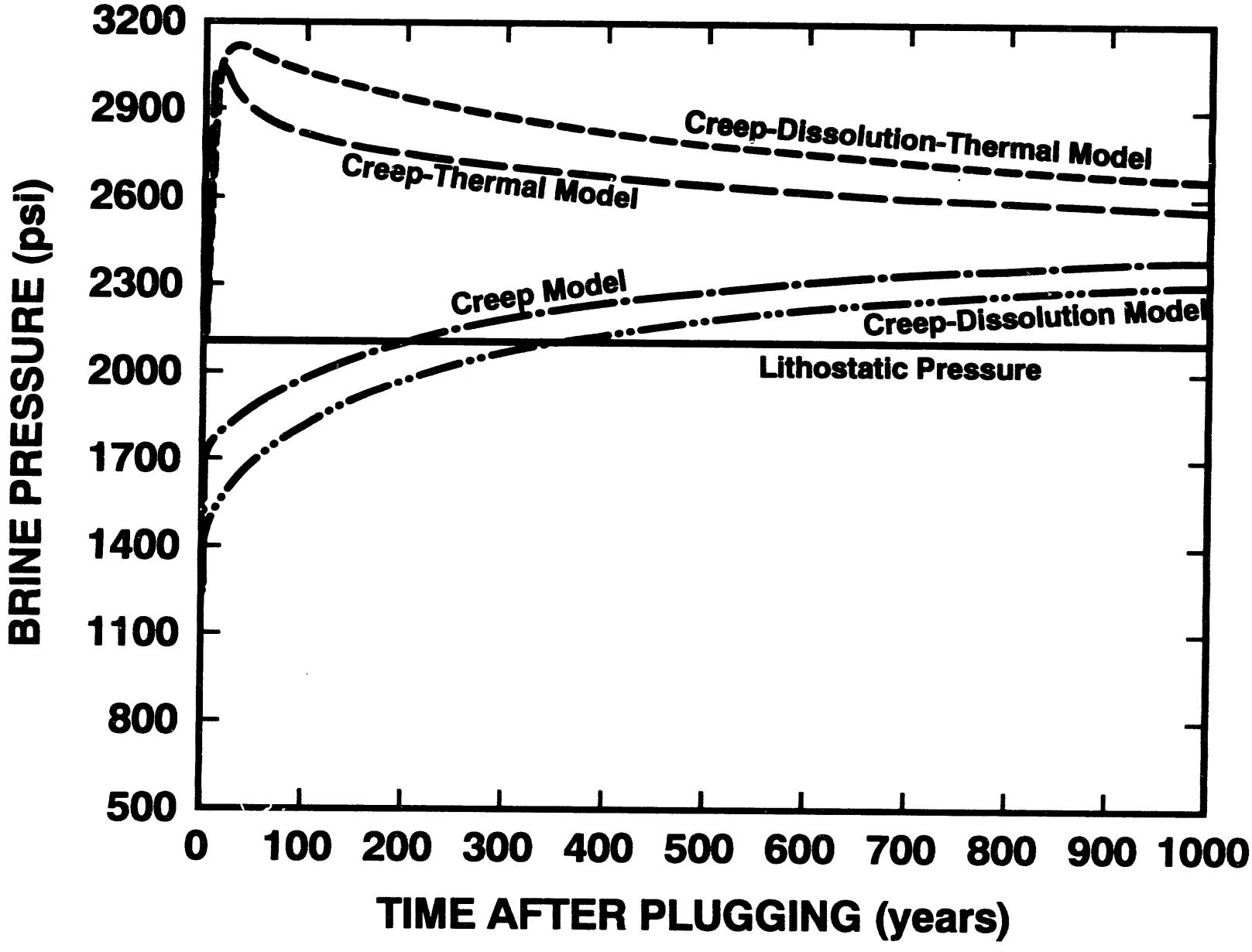

Figure 3-7. Coupled Model Predictions (0 to 1000 yrs) of Brine Pressure at Casing Seat.

4.0 PLUGGED CASING ANALYSES

4.1 Introduction

The mechanical behavior of a plugged borehole casing seat is predicted in this Chapter using the geothermally heated brine pressure history from the Chapter 3 cavern analyses. The previous cavern analyses coupled thermal, dissolution, and creep models in various combinations to estimate potential brine pressure histories that may be expected at a casing seat following cavern sealing. The thermal-creep model with no dissolution predicted the quickest loading at the casing seat. Including dissolution with thermal heating of the brine resulted in a slightly higher peak brine pressure, but the pressurization rate was substantially reduced. Since creep is load rate dependent, the predicted brine pressure history from thermal model (without dissolution effects) is used as input into finite-element analyses presented here. Faster loading rates tend to fracture salt more easily, than slower pressurization rates that allows more time for the salt to creep. The effect of load rate on wellbore fracturing was examined by Gniady and Ehgartner (1993) for SPR salts.

The access well to the cavern was plugged with cement following 30 years of cavern operation. The plug in this case is simply that extends from the casing seat upwards a significant distance into the casing.

4.2 Finite-Element Model

The geometric model consisted of a 20-inch (O.D.) steel casing cemented into a 26-inch diameter hole in salt. The interior of the casing was modeled as a pressure boundary condition to simulate oil and brine pressures prior to sealing, and later as a cement plug. The salt, steel, and cement were simulated using the models and properties as described in Chapter 2.

The finite-element mesh for the problem is shown in Figures 4-1a,b. The problem was idealized as axisymmetric with a vertical axis of rotation located on the left side of the mesh along the centerline of the borehole Rollered boundary conditions were applied to the right side and lower portion of the mesh to constrain salt flow perpendicular to the

outer and lower boundaries. These boundaries are assumed to be sufficiently removed from the plug that its response should not be effected by the constraints placed on them. Lithostatic pressure was applied to the materials, resulting in an overburden pressure of 2110 psi at the casing seat. Consistent with the analyses in Chapters 3 and 5, this approximates a depth of approximately 2400 ft.

The lithostatic pressures were assumed to be constant throughout the simulation time. In reality, they will probably increase in the vicinity of the casing seat as the cavern pressurizes over lithostatic pressure, because the casing set is typically only 100 ft above the roof of the cavern. This should result in larger compressive stresses in the casing and plug, and less long-term borehole creep than predicted by assuming a constant lithostatic pressure. In regard to this assumption, the analyses conclusions should be conservative.

For the initial 29.75 years of the calculation, a constant pressure of 1560 psi was applied to the interior of the steel casing and along the uncased borehole wall. The pressure is typical of what may be expected at a casing seat depth of 2400 ft during the operational period of a SPR cavern with an oil/brine interface near the bottom of the cavern (4500 ft). At 29.75 years, the pressure was dropped to 1250 psi to simulate brine pressure following the complete withdrawal of oil from the cavern in preparation for sealing. This pressure was maintained to 30 years. The above pre-plug portion of the calculation is necessary to help establish the correct stress state for the casing seat and surrounding salt at the time of plugging.

The casing was simulated as plugged at 30 years by placing cement elements inside the casing and applying the thermal-creep pressure history. The pressure history from the thermal-creep model of a sealed cavern (pressure due to geothermal heating of brine and creep closure of cavern) was applied horizontally to the uncased portion of the borehole below the plug and vertically to the plug and casing seat surfaces. Figure 4-2 reproduces, from Chapter 3, the pressure history. As discussed in Chapter 3, the brine was assumed to geothermally heat from an initial emplacement temperature of 107 °F to the average in situ temperature of the salt along the cavern wall (124 °F). Temperature changes of the salt and casing materials are not simulated in the analyses.

The brine pressure history was modeled as a step function with pressure increments/decrements of approximately 100 psi. The effect of incremental loading on the analyses results is small, but nonetheless sometimes noticed when examining the results of

the analyses. Because of creep and thermal heating of the brine, the pressure quickly exceeds lithostatic pressure (2110 psi) at 2.2 years after plugging. The brine pressure reached a maximum of 3060 psi at 16.5 years after plugging, followed by a gradual depressurization to 2780 psi at 170 years after plugging. The calculation was stopped at this time, thus capturing the peak borehole loading and load reversal. After 170 years, the brine pressures continue to decrease in time until the cavern reaches equilibrium pressure. As discussed in the previous chapter, as long as the cavern has a vertical dimension, theoretically the cavern brine pressure can not be in equilibrium with salt pressure because of differences in density (and hence pressure gradients) between brine and salt. However, for purposes of this report where the vertical cavern dimensions do not appreciably change, equilibrium can be assumed to equal the average lithostatic pressure along the cavern wall. This results in a pressure of approximately 2550 psi at the casing seat.

4.3 Results

It is important to identify any areas of tensile stresses in the results. The presence of tension in salt, cement, or at any material interface would indicate potential material fracturing or separation. This could create a flow path for the brine if it were to propagate.

Tensile stresses were not predicted at any location or time during the simulation. As a result of over-pressurizing the borehole (fluid pressures greater than lithostatic), the borehole temporarily enlarged in the vicinity of the casing seat and the compressive radial stresses decreased to a minimum of approximately 1030 psi at the casing seat. The minimum compressive stress occurred in the cement annulus between the steel casing and salt at 30 years after plugging. Figure 4-3 shows the predicted radial and hoop stress in that area. The first 30 years on the plot represent the operational phase of the cavern. At 29.75 years, the cavern oil was withdrawn and replaced with brine, and the cavern was plugged at 30 years. The effect of each of these operations on the casing seat stress is noticeable.

The hoop stress shown in Figure 4-3 is the maximum (most compressive) hoop stress predicted by the analysis, whereas the radial stress represents the minimum (or least compressive) stress. The hoop stress follows a path similar to the radial stress, where both initially decrease after plugging but eventually become more compressive with time.

The maximum predicted hoop stress in the cement approximately equals the estimated unconfined compressive strength of the cement (3625 psi) at the time of plugging. However, since the cement is under approximately 2000 psi of confinement at that time, the cement should be significantly stronger than the unconfined compressive strength.

The stresses predicted in the cement depend upon the initial stress state assumed for the cement. As mentioned earlier, all of the materials in the analysis were initially assigned a stress equal to lithostatic pressure. However, the initial stress state of the cement can depend upon the emplacement technique and specific formulation. A typical plug emplacement procedure would use a weighted fluid such as drilling mud to counter the brine pressures and thus stabilize the fluid motion in the casing. This would stress the cement during emplacement. The expansive characteristics of certain classes of cement, typically used in sealing, provide an additional compressive stress while hardening. A similar procedure is used when cementing a casing into place. A cement shoe is lowered through the drilling mud to the casing seat and the cement is forced up through the annulus between the casing and the salt. As such, the cement sets under pressure and is further pressurized due the salt creep loading that may occur. It should be noted that in addition to the expansive cements, salt creep, and emplacement procedures, the creep of cement helps to establish lithostatic pressure in the cement.

If the cement plug was not prestressed, then the stresses in the plug may become tensile with time. This occurs because the steel casing is predicted to enlarge by a maximum of 0.003 in. The stresses (radial and hoop) of an initially unstressed plug approach a maximum tensile stress of 610 psi before starting to become more compressive as the casing diameter contracts. These tensile stresses may approach the tensile strength of the cement.

The borehole deformations in Figure 4-4 are grossly exaggerated to show the predicted shape of the over-pressurized borehole 100 years after plugging. As shown in Figures 4-1a,b and in this figure as well, the unmagnified deformations of the plugged casing are very small. The predicted radial borehole deformations at the bottom of the uncased borehole and at the casing seat are shown in Figure 4-5.

Figure 4-5 shows that for the initial 30+ years, the uncased hole closes by approximately 0.15 in (twice the radial wall displacement). During this time the pressures in the borehole are less than lithostatic as cavern sealing has not yet occurred. The effect of the reduced

borehole pressure during oil drawdown, results in a noticeable increase in borehole closure. After plugging, over-pressurization in the uncased portion of the hole enlarges it by 0.27 in to result in a net borehole expansion of 0.12 in at 200 years. The uncased portion of the borehole continues to expand after 200 years at a rate of approximately 2.4×10^{-4} in/yr. In comparison, the radial displacements of the salt at the casing seat are much smaller in magnitude.

The borehole at the casing seat enlarges by a maximum of 0.008 in after plugging. Although the borehole wall at the casing seat enlarges after plugging, it starts to close after approximately 30 years of plugging. In trend, the deformations at the casing seat are similar to the predicted radial and hoop stresses at the casing seat (Figure 4-3), because the sealing materials were modeled as elastic materials where deformation is linearly related to stress.

Figure 4-6 shows the predicted radial and hoop stresses for the uncased portion of the borehole (remote from the casing seat). The radial stress component represents the brine pressure on the borehole wall. The brine pressure increases for 16.5 years after plugging and exceeds lithostatic pressure 2110 psi at 2.2 years after plugging. The hoop stress was reduced to approximately 1380 psi at 1.9 years after plugging and increased thereafter in compression. This behavior is attributed to the viscoplastic nature of salt. Even though the borehole is predicted to expand, the hoop stresses remain compressive. This result has been investigated in some detail by Gniady and Ehgartner (1993), who showed the minimum compressive stress to be a function of borehole pressurization. Therefore, the rapid loading and high pressures imposed by using the creep-thermal results from the suite of cavern analyses make the plug predictions conservative (i.e. producing the least compressive plug stresses).

Several additional analyses were performed to evaluate the sensitivity of the above results to other possible casing seat geometries and conditions. The same finite-element mesh as shown in Figures 4-1a,b was used in all the analyses. The materials assigned to portions of the casing and cement elements were varied. Specifically, one analysis replaced the cement annulus between the steel casing and salt with salt. Therefore, a salt corner results at the casing seat, formed by the two different borehole diameters in the cased and uncased portions of the borehole. The same size steel casing was modeled but it directly contacts the salt. The minimum radial stress was predicted to be approximately 1930 psi compressive. Another analysis, modeled the cement annulus between the steel casing and

salt as steel. This simulated a much thicker casing in direct contact with the salt with the same size borehole in the cased and uncased portions of the borehole. The minimum radial stress predicted to act against the casing was 1520 psi compressive. A third analysis replaced the outer ring of steel casing elements with a very soft elastic material (E= 15 psi) to simulate a corroded outer surface on the casing and a weak bond between the casing steel and cement. As a result, the effective thickness of the steel casing was reduced by one-third. The predicted radial stresses dropped to a minimum of 1870 psi compressive and practically all of the radial displacement (up to 0.008 in enlargement) was predicted to occur across the soft interface. Although there was some difference in the stresses predicted, dependent upon specific casing seat geometry and materials, the stresses at the casing seat and in the uncased borehole remained compressive and the borehole wall at the casing seat eventually starts to close after having enlarged.

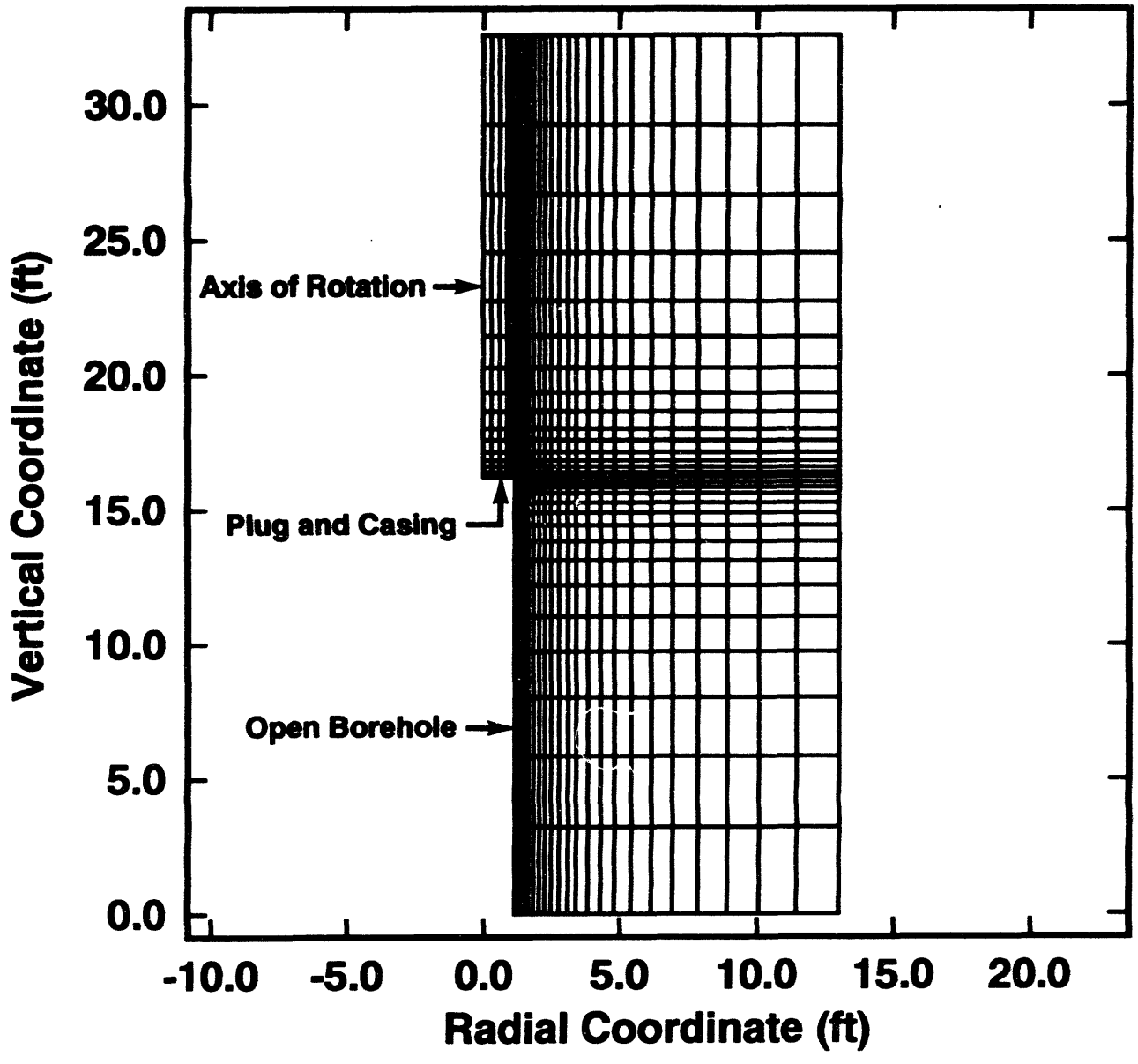

Figure 4-1a. Finite-Element Mesh of Plugged Casing and Open Borehole (100 years after plugging).

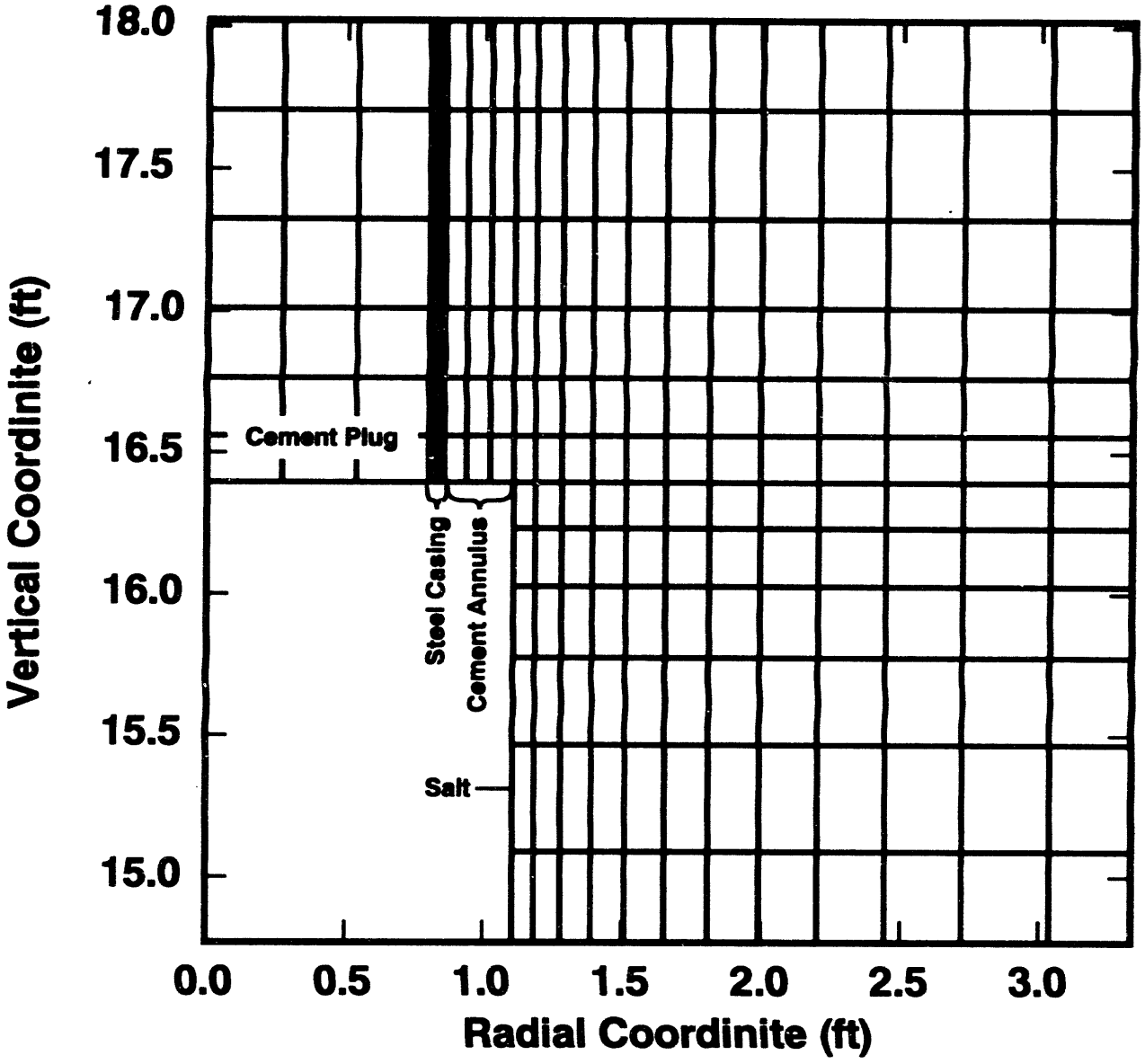

Figure 4-1b. Enlarge Portion of Finite-Element Mesh at Bottom of Plug (100 years after plugging).

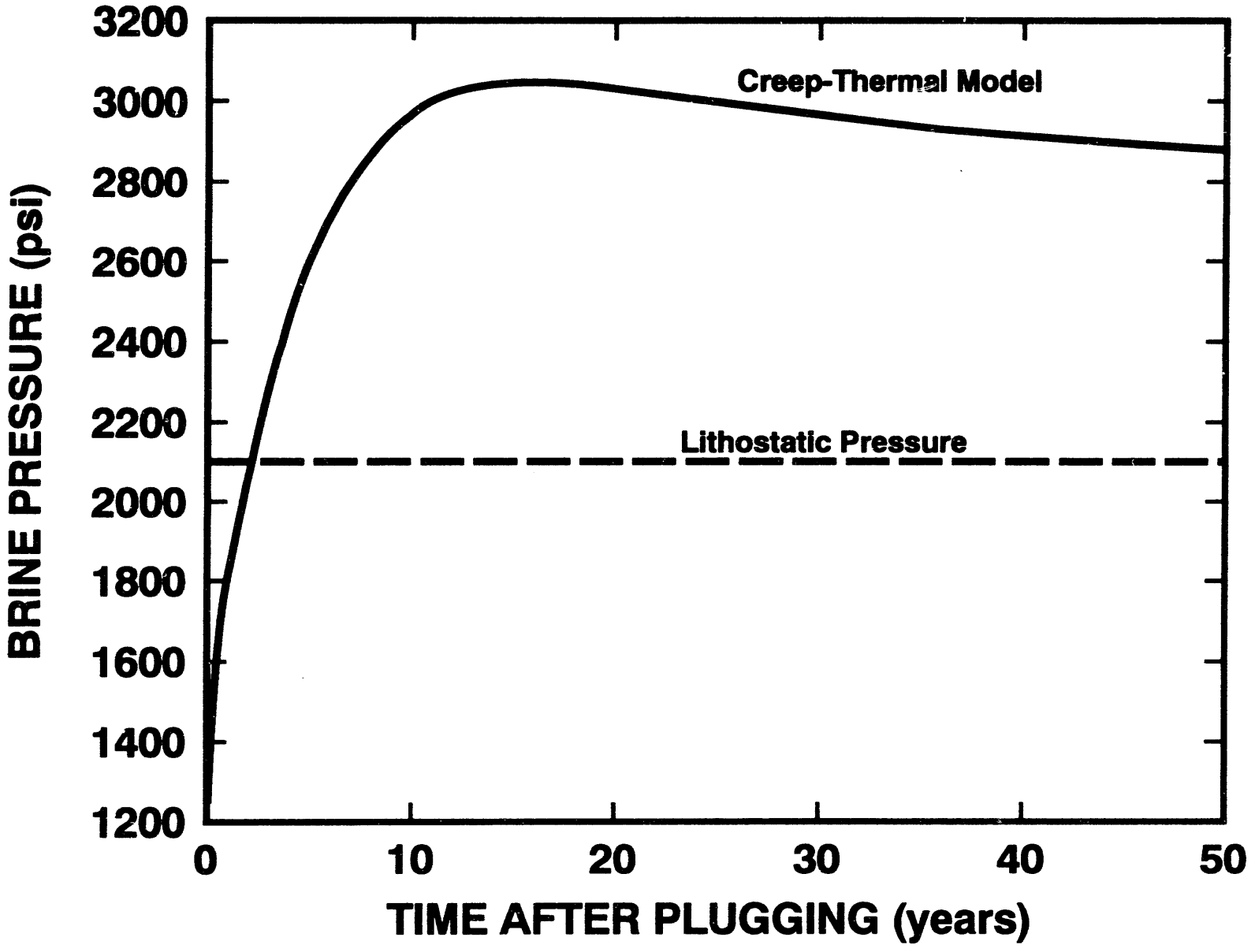

Figure 4-2. Thermal-Creep Pressure History Used in Analyses.

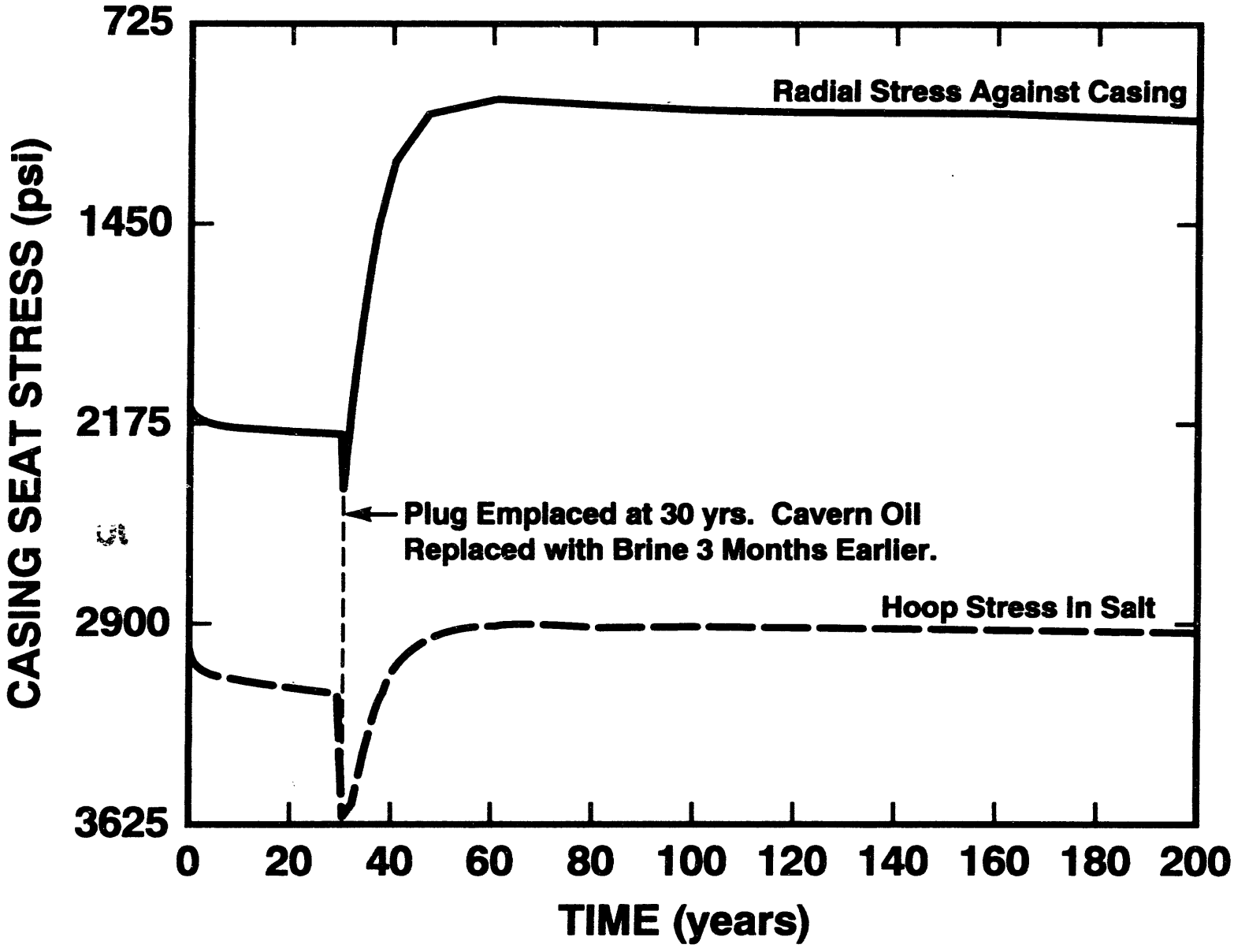

Figure 4-3. Predicted Radial and Hoop Stresses Acting Against Bottom of Casing.

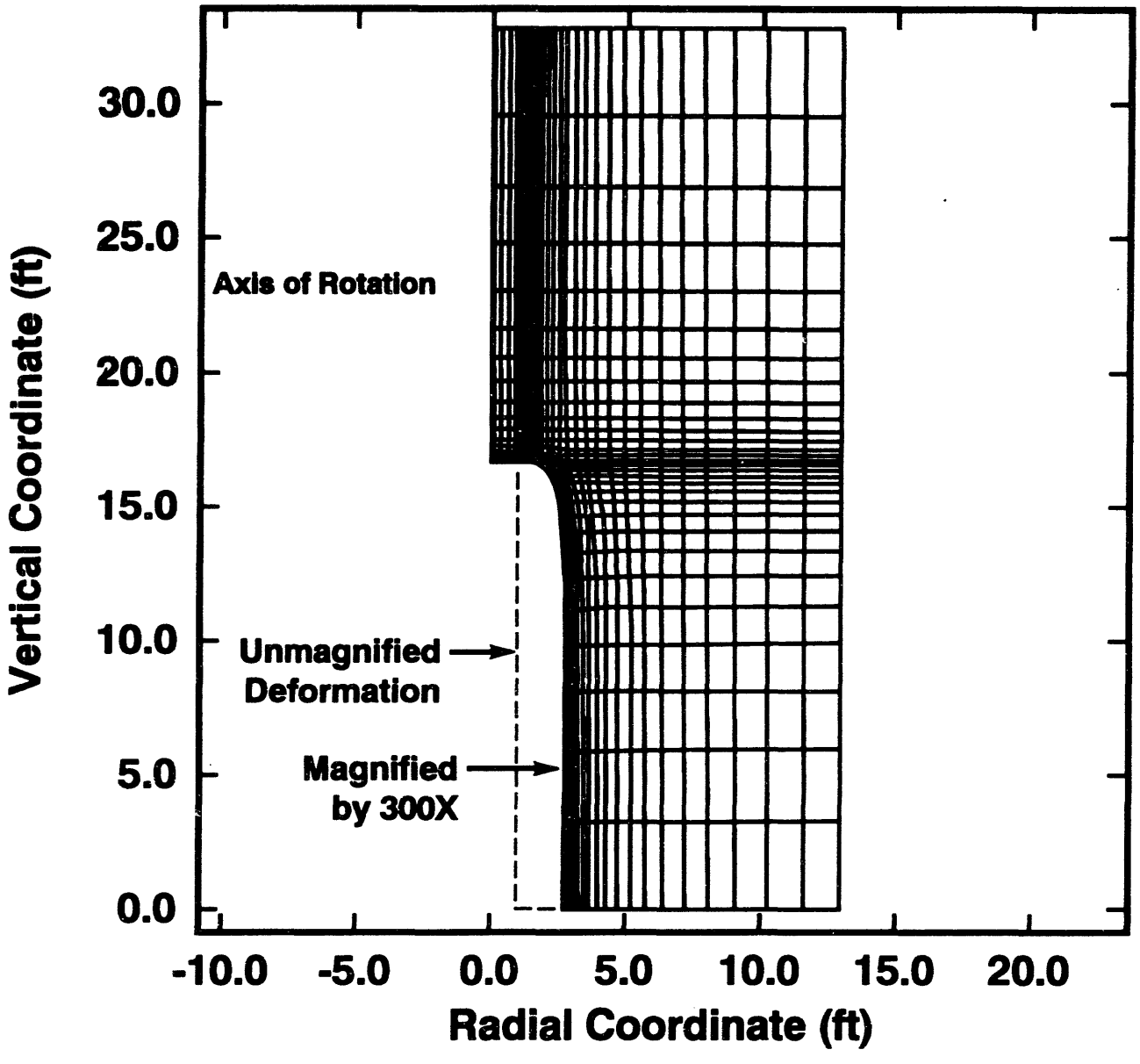

Figure 4-4. Deformed Borehole Shape Exaggerated by 300 Times at 100 years *after plugging.*

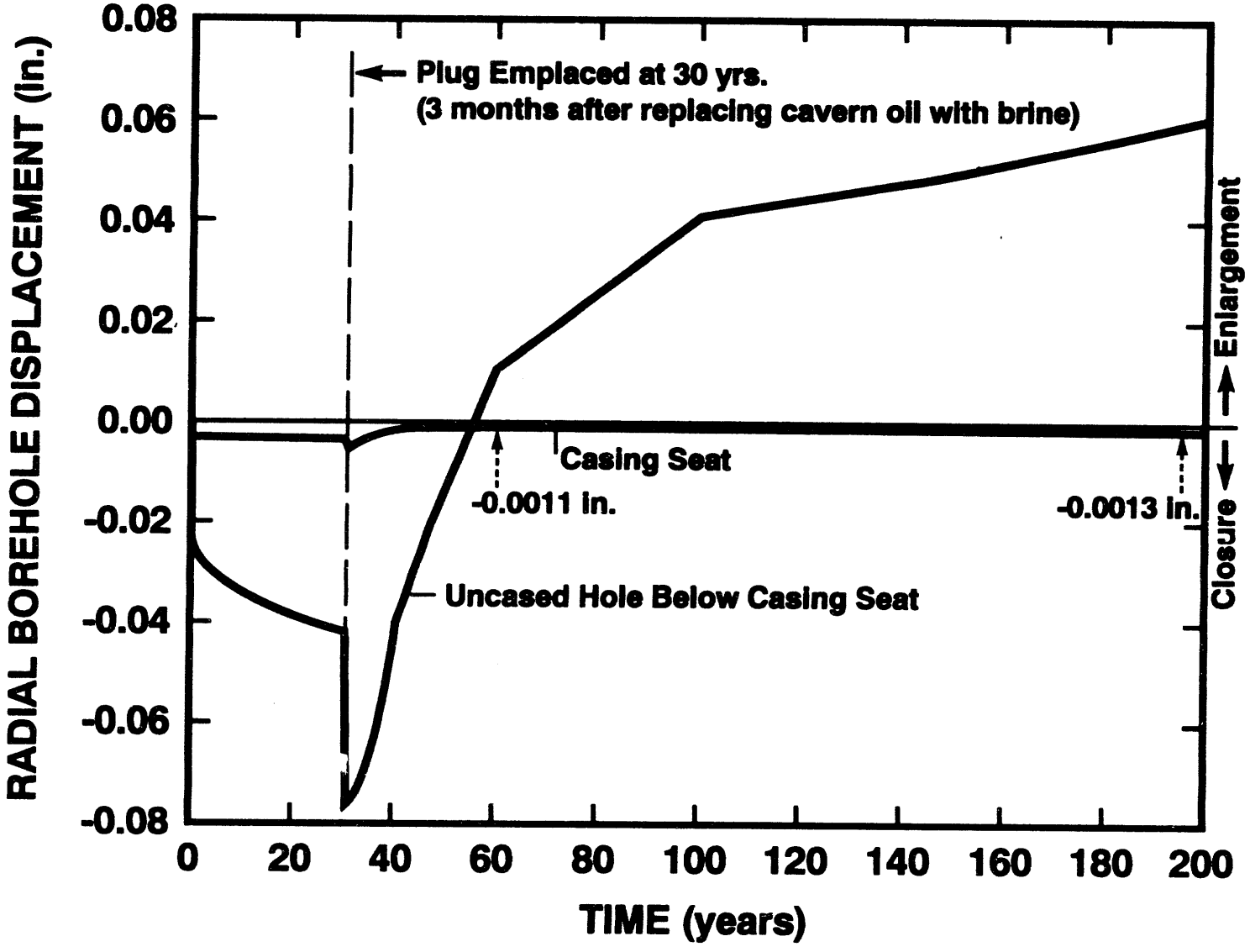

Figure 4-5. Predicted Radial Borehole Displacements for Open Uncased Hole and at Casing Seat.

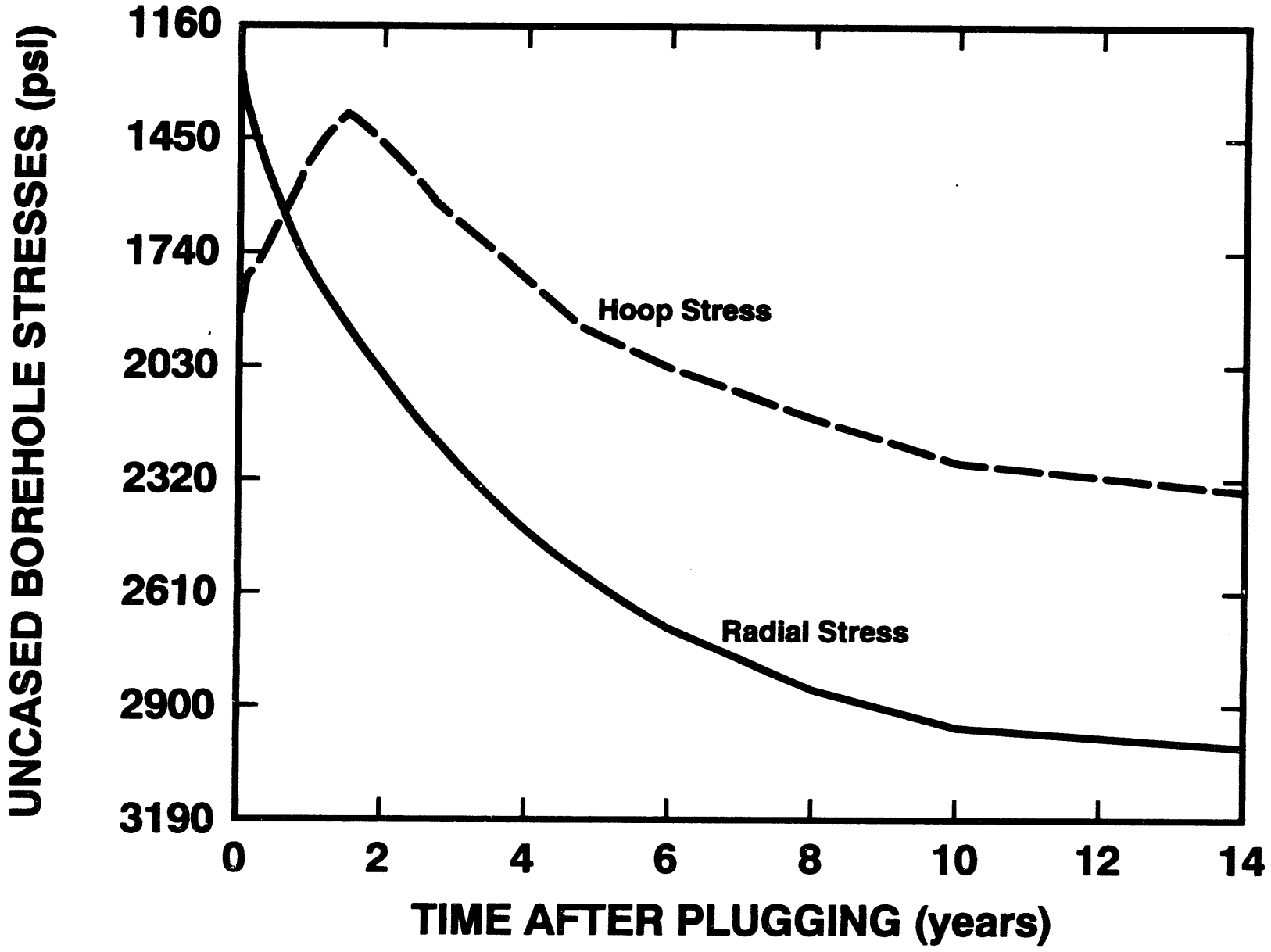

Figure 4-6. Predicted Radial and Hoop Stresses in Uncased Borehole Below the Casing Seat After Plugging at 30 Years.

5.0 CASING INTERFACE ANALYSES

5.1 Introduction

After cavern sealing and abandonment, the fluid at the casing seat is predicted to pressurize above lithostatic pressure. The fluid could pressurize any pre-existing cracks or interfaces along the casing which may have been formed due to a poor cement job, extremes in operating pressures, or perhaps material degradation or casing corrosion. This report evaluates the mechanical response of a cement/salt interface pressurized in excess of lithostatic pressure.

The interface was composed of a lower and upper portion. The lower portion of the interface was assumed to be filled with pressurized fluid in an attempt to determine under what conditions the interface is expected to propagate or grow. The upper portion of the interface was modeled as both an unfilled interface providing no resistance to separation (unbonded or missing cement) and also as a cement filled interface with bonding.

The previous cavern analyses (Chapter 3) coupled thermal heating of brine, salt dissolution, and cavern creep models in various combinations to estimate potential brine pressure histories that may be expected at a casing seat following cavern sealing. The thermal-creep model assuming no salt dissolution predicted the quickest loading at the casing seat. If no thermal heating of the brine occurred, then the pressure magnitudes and rates would be significantly reduced. The sensitivity of these pressure histories to the response of the plug/salt interface is examined in this chapter.

5.2 Finite-Element Model

Two analyses were initially performed. The first assumed the upper portion of the interface to be unfilled, and therefore the interface was free to separate without resistance. The second calculation assumed the upper portion of the interface to be cement filled. For these two analyses, the thermal-creep pressure history was used.

A third analysis was performed similar to the second except that the lower portion of the

interface was loaded with the predicted brine pressure history assuming no thermal loading of the brine. This pressure history resulted from salt creep only and lacked the thermal drive used in the first two analyses. As such the predicted pressurization rate and maximum pressure was much lower. This analysis will quantify potential improvements to the interfacial stress state if the brine injected into the cavern prior to plugging is allowed to thermally stabilize with the geostatic temperatures.

The geometric model consisted of 20-inch steel casing (O.D.) cemented into a 26-inch hole in salt. Initially, the entire geometry, including both portions of the interface, and fluid pressure was at lithostatic pressure. Afterwards, the wellbore and lower portion of the salt/cement interface (0.1 inches across) was pressurized in excess of lithostatic pressure.

The unfilled interface was simulated as an elastic material with an extremely low modulus (15 psi). As such, the material provided no resistance to enlargement or opening of the interface and the stress across the interface remained essentially unchanged at lithostatic pressure throughout the calculation. The cement filled interface was also assumed to be elastic, but with the properties of cement, and therefore, can accept loading. The properties of the cement were unchanged with time. In reality, the cement along the interface may be altered with time due to material incompatibilities. The salt, cement and steel were modeled as defined in Chapter 2.

The finite-element mesh using quadrilateral elements is shown in Figure 5-1. The same finite-element mesh was used in both analyses. The problem was idealized as axisymmetric with a vertical axis of rotation located on the left side of the mesh. Rollered boundary conditions were applied to the right side and lower portion of the mesh. This results in a plane of symmetry across the bottom of the mesh. Because of symmetry, the lower portion of the interface represents a total length of 7 inches, and it surrounds the casing cement to form an annular shape with a thickness of 0.1 inch. Because the interface length is large relative to its thickness, the stresses at the boundary between the upper and lower portions of the interface (top of the fluid pressure boundary) should not be effected by its length. The outer boundary of the mesh is assumed to be sufficiently removed from the interface that interfacial behavior should not be effected by constraints placed on the outer edge of the mesh.

An overburden pressure of 2110 psi was applied to the upper surface of the mesh. Initial

stresses of equal magnitude were uniformly applied throughout the model. The lithostatic pressures were assumed to be constant throughout the simulation time. In reality, they will probably increase in the vicinity of the casing seat as the cavern pressurizes over lithostatic pressure, because the casing seat is typically only 100 ft above the roof of the cavern which also pressurizes. This will reduce the pressure differential between the fluid and the salt, resulting in less deformation than predicted by assuming a constant lithostatic pressure.

The pressure history from the thermal-creep and creep only models of a sealed cavern (Chapter 3) was applied to the lower portion of the interface starting at lithostatic pressure (2110 psi). In the case of where the upper portion of the interface was simulated as unfilled, fluid pressure was applied to the sides of the lower portion of the interface. For the cemented interface, fluid is also assumed to contact and pressurize the bottom edge of the cement bond. The pressure history was modeled as a step function with pressure increments/decrements of approximately 50 psi. As a result of the incremental loading, the analyses results are stepped.

The thermal-creep pressure history from Chapter 3 increased the interface pressure from lithostatic pressure (2110 psi) to a maximum of 3060 psi at 14.3 years, followed by a gradual depressurization to 2830 psi at 100 years. The calculations using the thermal-creep loading were stopped at this time, thus capturing the peak interface loading and load reversal. For the thermal-creep model, the brine was assumed to pressurize as a result of thermal heating of the brine from an initial emplacement temperature of 107 °F to the average in situ temperature of the salt along a typical SPR cavern wall (124 °F).

The creep only pressure history results in a gradual pressure increase from lithostatic pressure to the estimated creep equilibrium pressure for the cavern. Equilibrium is estimated to equal the average lithostatic pressure along the cavern wall. For a typical SPR cavern (2000 ft high, roof at 2500 ft), the brine pressure at the casing seat will be approximately 2550 psi when approaching cavern equilibrium. As discussed in Chapter 3, equilibrium may never be achieved but only approached. Extrapolating from the results provided in Chapter 3, cavern equilibrium is defined at approximately 1800 years after sealing for a cavern that is pressurized solely due to creep.

Figure 5-2 compares the predicted casing seat pressures for each model and shows the impact of heating on the predictions. The figure also shows the estimated lithostatic and

brine equilibrium pressures at the casing seat.

5.3 Results

The emphasis in examining the results was to look at the displacements and stresses across the interface directly ahead of the fluid boundary. For the unfilled interface, displacements that predict interface separation at the fluid boundary imply potential fluid propagation along the interface. The presence of tension in salt, cement, or across any interface would imply potential fracturing or interface separation. Separation along the interface could lead to pressurization of an even larger portion of the interface. The process may continue to propagate upward along the casing eventually forming a leak path from the cavern.

Figures 5-3 shows the displacement vectors and deformed shape of the unfilled interface (magnified by 10) after 100 years of pressurization above lithostatic pressure for the unfilled interface. The pressure history used in the analyses assumed thermal-creep loading of the brine. It is obvious that the unfilled portion of the interface is predicted to separate above the pressurized portion and would likely pressurize as a result of upward fluid migration. This result is expected because the applied brine pressure exceeds lithostatic pressure and there is no resistance to separation. A similar behavior is expected if the applied pressures were based on only creep loading of the brine, but the magnitudes of displacement would be less at a given time.

Figure 5-4 plots the displacement vectors for the cemented interface. In comparison to the unfilled interface analysis, salt flow associated with the cemented interface is quite different. The salt is predicted to flow towards the cemented interface, rather than away from it. This results in a much smaller enlargement at the boundary between the upper and lower portions of the interface.

Figure 5-5 shows the cemented interface to separate by a maximum of only 1.4×10^{-4} in after 10 years, whereas the unfilled interface is predicted to separated by 0.010 in at 10 years and continue to open thereafter. The cemented interface starts to close after 10 years.

Figure 5-6 shows the predicted stress history across the interface at the start of the cemented interface. These stresses represent the minimum (least compressive) pressures

predicted across the interface. Because the cemented interface is initially predicted to separate, the stress across the interface decreases from its initial lithostatic pressure. This drop in pressure causes the salt to flow in that direction, i.e., toward the cemented interface. The stress across the interface is predicted to go into approximately 580 psi of tension at 10 years, before recompressing. Tension is only predicted at the start of the cemented interface. All other areas in the cement and salt are predicted to be in compression. The tensile stress across the interface approximately equals the estimated tensile strength of the cement (600 psi). The steps in the Figure result from the pressure history being applied as a step function. A sudden increase or decrease in stress is the elastic response of the interface to the step loading of the brine.

Figure 5-7 plots the minimum predicted interface pressure across a cemented interface where the applied fluid pressure history was from creep only loading. The absence of a thermal load on the cavern brine results in a much slower applied pressure rate. Consequentially, the results are examined over a 2000 year period instead of the 100 years used above. In contrast to the analysis which also included thermal loading of the brine, the creep only load results in a compressive interface. The predicted interface pressure is least compressive (870 psi) during the final load step at 1800 years when cavern equilibrium pressure is reached. After that, the interface pressure becomes more compressive in time.

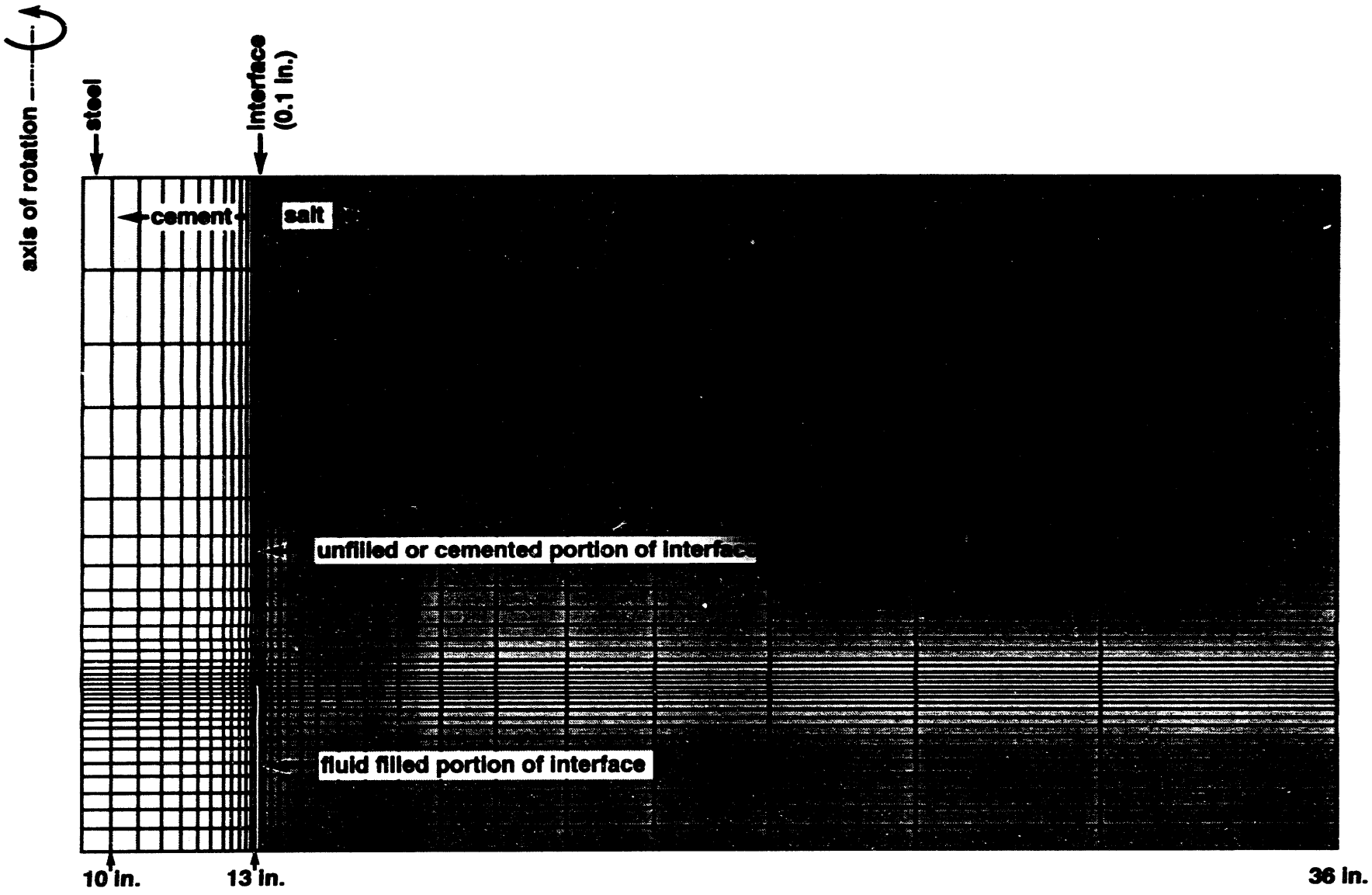

Figure 5-1. Axisymmetric Finite-Element Mesh Showing Steel Casing, Cement Annulus, Interface, and Salt. Open portion of interface is pressurized. Top portion of interface is simulated as 1) unfilled (free to separate) and 2) as cemented.

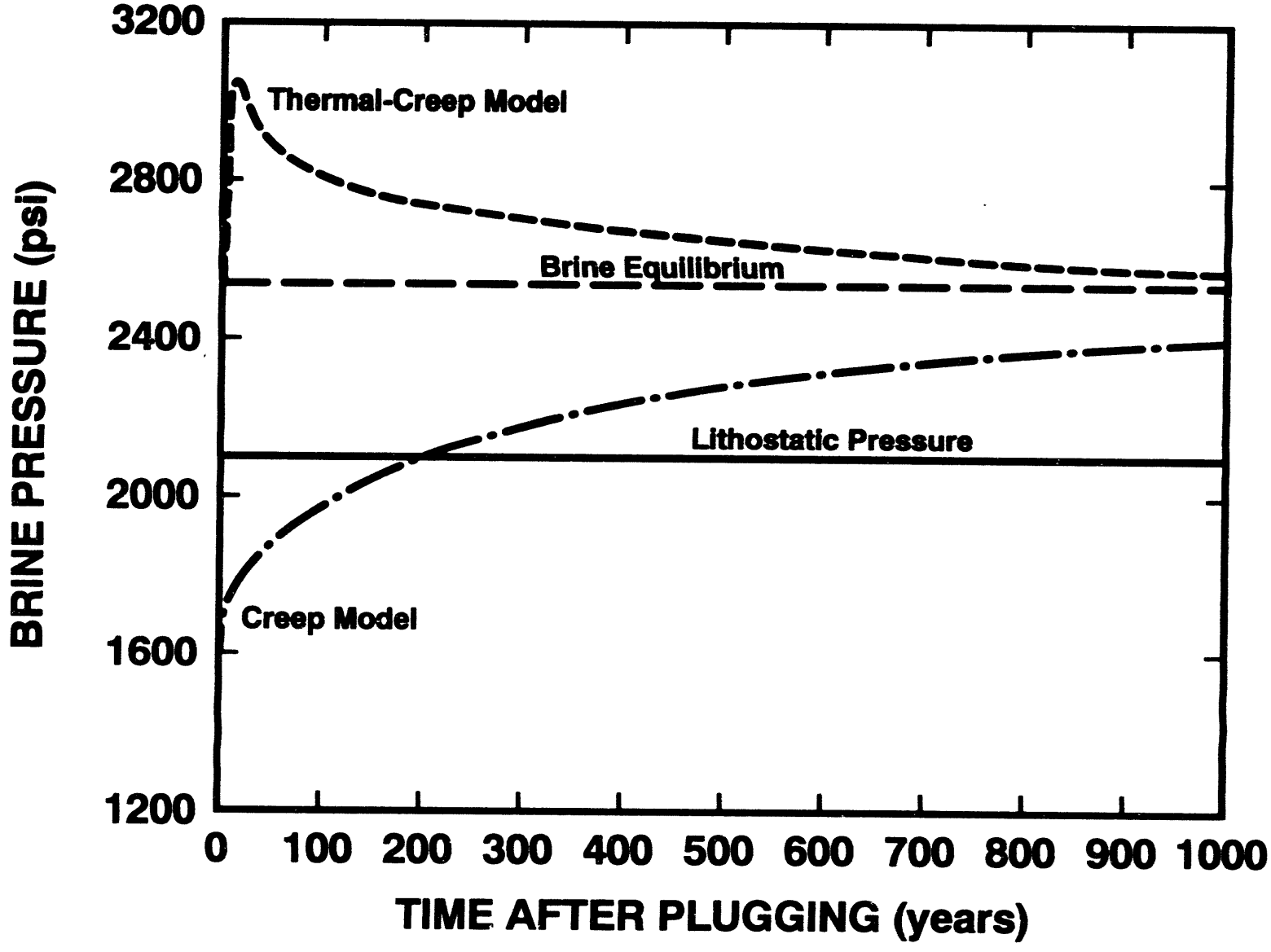

Figure 5-2. Predicted Brine Pressure Histories at The Casing Seat From Coupled Thermal-Creep and Creep Only Models. Also shown are the estimated lithostatic and brine equilibrium pressures at the casing seat.

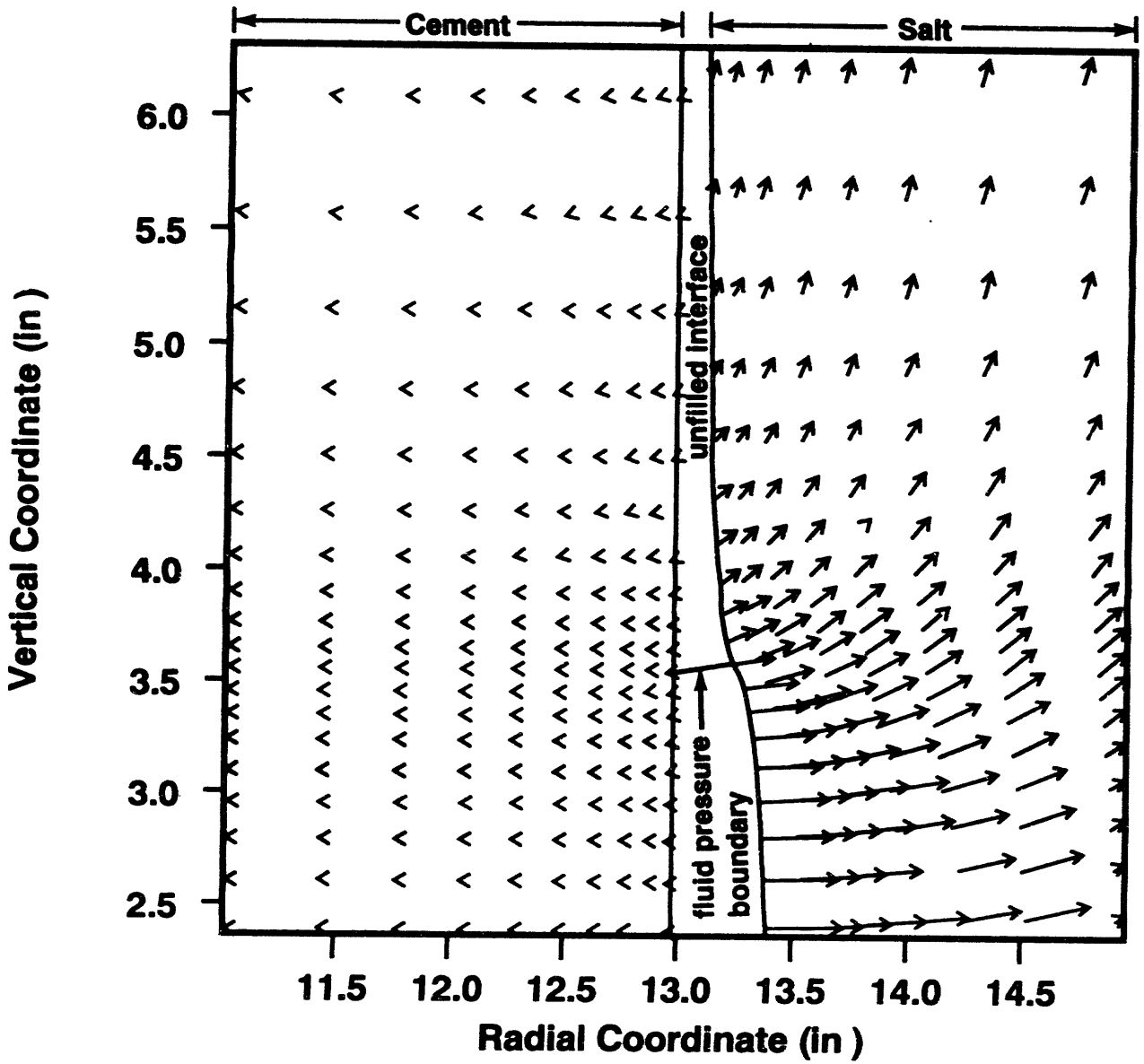

Figure 5-3. Displacement Vectors (Magnified by 10) for Unfilled Interface at 100 Years Showing Enlargement and Flow of Salt Away From Interface. The thermal-creep pressure history was applied to the cement and salt below the fluid pressure boundary.

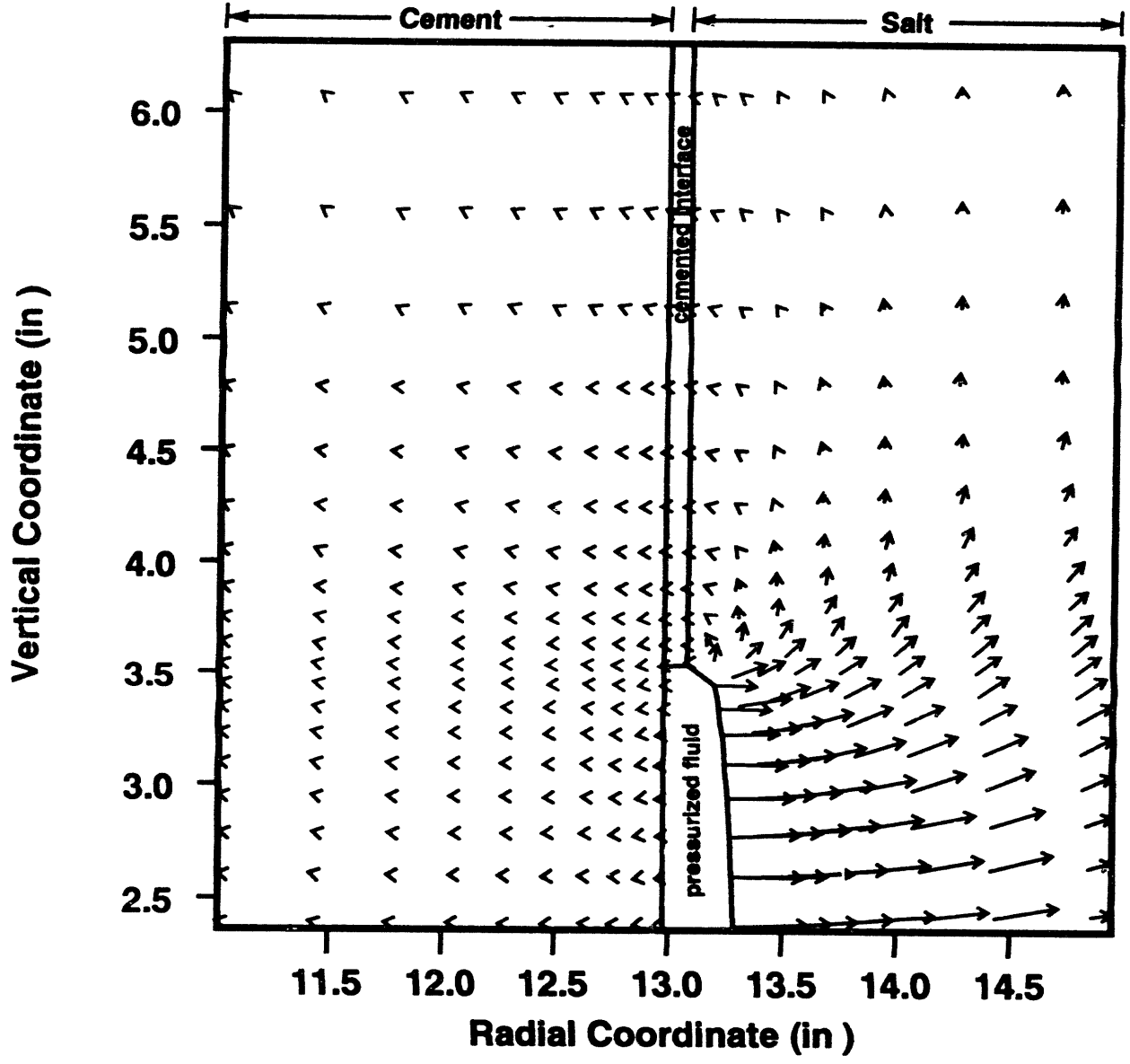

Figure 5-4. Displacement Vectors (Magnified by 10) for Cemented Interface at 100 Years Showing No Discernible Enlargement and Flow of Salt Toward Cement Portion of Interface. The thermal-creep pressure history was applied to the fluid filled portion of interface.

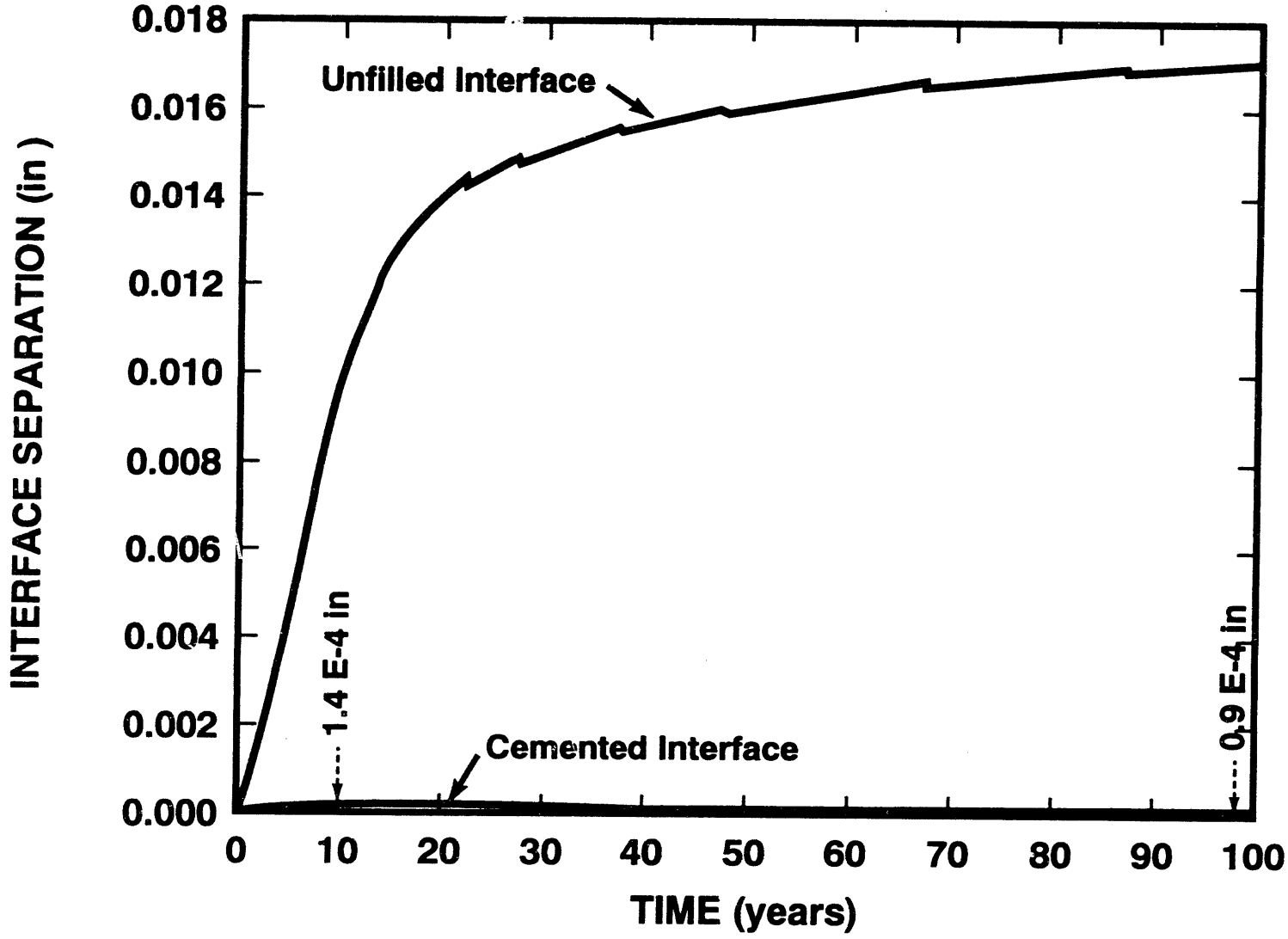

Figure 5-5. Predicted Interface Separation at Fluid Level for Unfilled and Cemented Interfaces Showing Continual Enlargement for Unfilled Interface and Eventual Closure of Cemented Interface. The thermal-creep pressure history was applied to the fluid filled portion of interface.

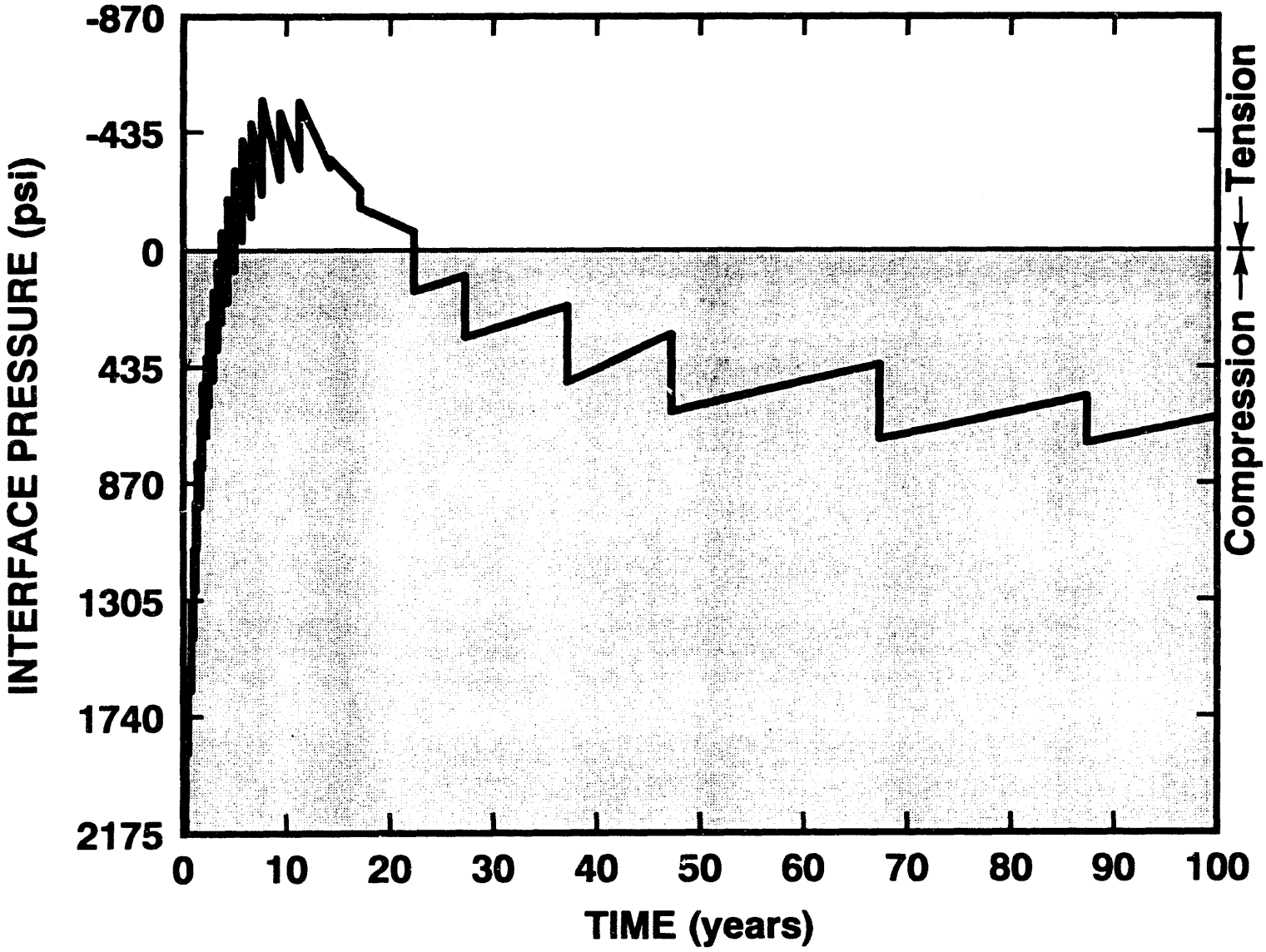

Figure 5-6. Minimum Predicted Interface Pressures Across Cemented Interface Showing Interface to Initially Decompress Into Tension and Then Recompress into Compression. Steps in interface pressure are an artifact of simulating the applied fluid pressure history (Thermal-Creep) Incrementally.

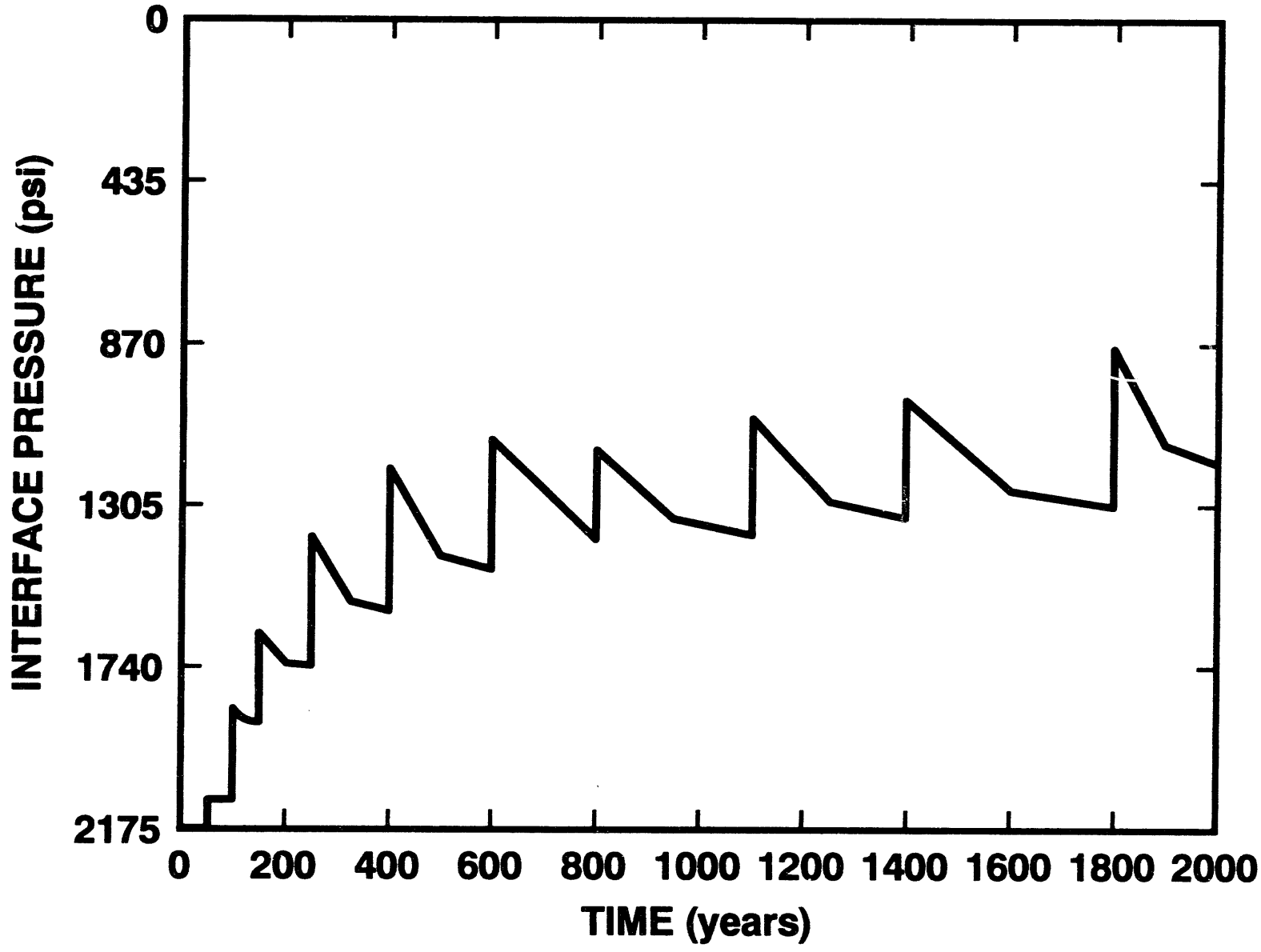

Figure 5-7. Minimum Predicted Interface Pressures Across Cemented Interface Showing the Interface to Remain in Compression. Steps in interface pressure are an artifact of simulating the applied fluid pressure history (Creep only) Incrementally.

6.0 CONCLUSIONS

Mechanical behavior and trends were established from the cavern, plugged casing, and casing/salt interface analyses presented in Chapters 3 through 5. The conclusions derived from these results and their significance to SPR cavern plugging are discussed below.

The cavern analyses showed that after plugging of the cavern, the brine pressure history at the casing seat is sensitive to the temperature and salinity of the brine at the time of sealing. The geothermal heating of brine had the greatest influence on brine pressurization after sealing. The predicted time for brine to reach lithostatic pressure at the casing seat was only a couple of years after sealing. In contrast, if the brine did not heat with time, two hundred years of cavern creep was required to pressurize the brine above lithostatic pressure at the casing seat. The maximum predicted brine pressures at the casing seat were much larger when geothermal heating of the brine occurred after sealing. The above results assume no salt dissolution after plugging of the cavern. When salt dissolution was included in the analyses, the time required for the brine at the casing seat to reach lithostatic pressure was nearly doubled.

Examination of the stress state surrounding the cavern showed that the cavern roof and wall stresses remained compressive after plugging. The worse condition was for the heated brine case which resulted in a relatively rapid pressurization of the brine in the cavern. The minimum predicted compressive stress in the salt surrounding the cavern was approximately 70 percent of lithostatic. After reducing in magnitude, the minimum compressive stress eventually became more compressive with time. The accumulated salt strain increased less than 1 percent over a 1000 year period after sealing due to small roof and wall displacements. Cavern deformation or creep rates are reduced after sealing due to the increased cavern brine pressures. The stresses and strains in the salt indicate that the cavern would be mechanically stable after plugging regardless of geothermal heating of brine, salt dissolution, and creep closure of the cavern.

The sensitivity of cavern brine pressures to thermal and dissolution effects provides an opportunity to engineer cavern abandonment and sealing options that would significantly 1) increase the time before the casing seat exceeds lithostatic pressure and 2) decrease the maximum fluid pressure exerted on the plugged casing seat. Higher brine temperatures

and lower salinities at the time a cavern is plugged results in a sealing advantages in that cavern pressures and pressurization rates are reduced, particularly during the early stages of abandonment.

Because the cavern fluid pressures were predicted to exceeded lithostatic pressure, a more detailed series of analyses were performed to examine the response of a plugged casing seat and the interface between the plugged casing and salt to pressures in excess of lithostatic. Fluid pressures in excess of the salt's lithostatic pressure could allow for fracturing or separation of material interfaces near the plugged casing seat as the wellbore enlarges.

The plug analyses suggest that the stresses near a plugged casing seat and in the uncased portion of the borehole below the plug will remain compressive even though the borehole enlarges due to the buildup in brine pressures in excess of lithostatic pressure. After plugging, the minimum compressive stress decreases to approximately 50 percent of lithostatic, but eventually become more compressive with time. The borehole diameter at the casing seat is predicted to enlarge up to approximately 0.008 in following plug emplacement, but eventually starts to creep close after approximately 30 years following plugging. Sensitivity analyses showed the predicted stresses to be slightly dependent upon the specific casing seat geometry and interface bonding. In all of the cases evaluated, the stress state remained compressive at all times. The predicted stress-deformation trends and magnitudes are desirable for ensuring long-term plug integrity and cavern sealing. Even though the plugged wellbore expands due to pressures in excess of lithostatic, the sealing materials and interfaces remain under compression and are not expected to mechanically fail or separate. This may prevent any leakage around the plug from occurring.

The above plugged casing analyses assume properly emplaced materials and no material degradation with time. A poor cement job near the casing seat or other mechanisms such as corrosion could result in a permeable interface between materials which could pressurize and eventually propagate upwards to form a leak path. This possibility was evaluated in the casing/salt interface calculations.

The interface analyses show that the propagation of a pre-existing crack along the interface of the casing and salt depends upon the condition of the interface and the brine pressure load. A good condition would imply that the interface is not materially degraded

and that a good bond strength exists at the interface. A degraded interface was predicted to open with time and thus allow fluid to propagate along that interface regarless of the pressure history assumed for the brine. The ability of an interface in good condition to propagate under a thermally driven brine pressure was questionable. The compressive interface stresses changed to tension for a short period of time (20 years) following plugging and approached the estimated tensile strength of the cement at that time However, the same interface remained under compression and most likely would not propagate when the thermal loading of the brine pressure was absent.

The above results suggest that leakage after cavern abandonment might be reduced or eliminated by grouting any pre-existing fractures or uncemented interfaces at the casing seat and by increasing the brine temperature in the cavern prior to sealing. Increasing the brine temperature to the average in situ temperature of the cavern can eliminate the subsequent natural thermal-pressure increase of the brine after plugging the cavern. A higher brine temperature may be obtained naturally by delaying installation of the seal and thus allowing the salt to heat the brine, or by artificially pre-heating the injected brine during oil withdrawal. Delaying sealing after oil withdrawal would remove the advantages due to dissolution.

In conclusion, the analyses presented in this report suggest that SPR caverns might be effectively sealed. This conclusion is based solely upon a limited number of mechanical finite-element analyses and no attempt was made to couple and simulate the effects of fluid permeation into the salt formation. As well, the finite-element model used in the evaluations has not been validated for this particular environment and field studies provide no consensus regarding the integrity of a sealed cavern or wellbore to pressures in excess of lithostatic (Gniady and Ehgartner, 1993). The specifics of the analyses presented in this report should not be interpreted as final sealing designs. Plugging and sealing of SPR caverns may entail more than just filling the interior of the borehole casings with cement. For example, multiple sealing materials with different purposes may be used to enhance sealing of SPR caverns. The analyses in this report do suggest that sealing and abandonment procedures should address: brine temperature and salinity, plug emplacement time and prestressing, and grouting at the casing seat as a minimum. These and other items, along with the information gained through the work of others in the national and international community, will contribute to a successful sealing and abandonment plan for SPR caverns.

7.0 REFERENCES

Ehgartner, B.L. 1990. Geomechanical Analyses in Support of the Waste Isolation Pilot Plant (WIPP), SAND90-0285, Sandia National Laboratories, Albuquerque, NM.

Ehgartner, B.L. 1991. Structural Analyses and Design of a Concrete Liner that Limit the Disturbed Rock Zone Around Underground Openings in Salt, SAND90-2702, Sandia National Laboratories, Albuquerque, NM.

Ehgartner, B.L. 1992. Effects of Cavern Spacing and Pressure on Subsidence and Storage Losses for the U.S. Strategic Petroleum Reserve, SAND91-2575, Sandia National Laboratories, Albuquerque, NM.

Gniady, C.T. and B.L. Ehgartner 1993. "Fracture Predictions for Over-Pressurization of Sealed Wellbores," SMRI Fall meeting, Lafayette, La.

Hoffman, E.L. 1992. Effects of Cavern Depth on Surface Subsidence and Storage Loss of Oil-Filled Caverns, SAND92-0053, Sandia National Laboratories, Albuquerque, NM.

Krieg, R.D. 1984. Reference Stratigraphy and Rock Properties for the Waste Isolation Pilot Plant (WIPP) Project, SAND83-1908, Sandia National Laboratories, Albuquerque, NM.

Kuhlman, P. and T. Russo, 1992. "Cavern Drawdown Analysis," unpublished SANSMIC calculation, Sandia National Laboratories, Albuquerque, NM.

Munson, D.E., 1979. Preliminary Deformation-Mechanism Map for Salt (with Application to WIPP), SAND70-0076, Sandia National Laboratories, Albuquerque, NM.

Munson, D.E. and K.L. DeVries, 1990. "Progress in Validation of Structural Codes for Radioactive Waste Repository Applications in Bedded Salt," Proc. of Geoval 90, Conference sponsored by SKI & OECD/NEA, Stockholm, Sweden.

Munson, D.E., K.L. DeVries, D.M. Schiermeister, W.F. DeYonge, 1992. "Measured and Calculated Closures of Open and Brine Filled Shafts and Deep Vertical Boreholes in Salt,"

Proceedings of 33rd U.S. Symposium on Rock Mechanics, June 1992, Santa Fe, NM.

Munson, D.E., A.F. Fossum, and P.E. Senseny, 1989a. Advances in Resolution of Discrepancies Between Predicted and Measured In Situ WIPP Room Closures, SAND88-2948, Sandia National Laboratories, Albuquerque, NM, February.

Munson, D.E., A.F. Fossum, and P.E. Senseny, 1989b. Approach to First Principles Model Prediction of Measured WIPP In Situ Room Closure in Salt, SAND88-2535, Sandia National Laboratories, Albuquerque, NM.

Preece, D.S. 1985. "Sealed Cavern Study", unpublished finite-element calculations, Sandia National Laboratories, Albuquerque, NM, 11/18/85.

Preece, D.S. and W.R. Wawersik, 1984. "Leached Salt Cavern Design Using A Fracture Criterion for Rock Salt," Proceedings of the 25th U.S. Symposium on Rock Mechanics, June, Northwestern University.

RE/SPEC, 1989. Documentation of SPECTROM-32: A Finite-element Thermomechanical Stress Analysis Program, RE/SPEC Inc., Rapid City, SD.

Russo, A.J. 1983. A User's Manual for the Salt Solution Mining Code, SANSMIC, SAND83-1150, Sandia National Laboratories, Albuquerque, NM.

Todd, J.L. 1991. "Projected Oil Temperature-- Bryan Mound Caverns 101, 110, and 112." Internal memo to file dated 8/16/91.

Tomasko, D. 1985. Preliminary SPR Thermal Model Description and Results for WH-11 and BM-4, SAND84-1957, Sandia National Laboratories, Albuquerque, NM.

Wawersik, W.R. and D.H. Zeuch, 1984. Creep and Creep Modeling of Three Domal Salts-- A Comprehensive Update, SAND84-0568, Sandia National Laboratories, Albuquerque, NM.

DISTRIBUTION

US DOE SPR PMO (7)
900 Commerce Road East
New Orleans, LA 70123
Attn: J. Kilroy, FE 443
J. Culbert, FE 4431
R. Myers, FE 4422
L. Rousseau, FE 443
M. Smith, FE 4411
TDCS (2)

US DOE SPR (2)
1000 Independence Avenue SW
Washington, DC 20585
Attn: D. Johnson
D. Smith

DynMcDermott Petroleum Operations (3)
850 S. Clearview Parkway
New Orleans, LA 70123
Attn: T. Eyerman
K. Mills
K. Wynn

RE/SPEC Inc. (1)
3824 Jet Drive
Rapid City, SD 57709
Attn: Joe Ratigan

Sandia Internal:
1561 H. S. Morgan, MS 0433
1561 E. L. Hoffman, MS 0433
6100 R. W. Lynch, MS 0701
6113 J. K. Linn (10), MS 0706
6113 S. J. Bauer, MS 0706
6113 B. L. Ehgartner (10), MS 0706
6113 T. E. Hinkebein, MS 0706
6113 P. S. Kuhlman, MS 0706
6113 R. V. Matalucci, MS 0706
6113 J. T. Neal, MS 0706
6113 J. L. Todd, MS 0706
6113 S. T. Wallace, MS 0706
6117 W. R. Wawersik, MS 0751
6117 D. S. Preece, MS 0751
6121 J.R. Tillerson, MS 1322
6121 D.E. Munson, MS 1322
7141 Technical Library (5), MS 0899
7151 Technical Publications, MS 0619
7613-2 Document Processing (10)
(for DOE/OSTI), MS 0100
8523-2 Central Technical Files, MS 9018

END

DATE
FILMED
3/28/94